Lawrence Berkeley National Laboratory
LBL Dissertations

Title
FAR-INFRARED GENERATION BY NONLINEAR OPTICAL INTERACTION

Permalink
https://escholarship.org/uc/item/7gj271r6

Author
Faries, Dillard Wayne.

Publication Date
1969-08-01

Thesis/dissertation

eScholarship.org Powered by the California Digital Library
University of California

UCRL-19059

cy. 2

RECEIVED
LAWRENCE
RADIATION LABORATORY
OCT 22 1969
LIBRARY AND
DOCUMENTS SECTION

FAR-INFRARED GENERATION BY NONLINEAR OPTICAL INTERACTION

Dillard Wayne Faries
(Ph. D. Thesis)

August 1969

AEC Contract No. W-7405-eng-48

TWO-WEEK LOAN COPY

This is a Library Circulating Copy which may be borrowed for two weeks. For a personal retention copy, call Tech. Info. Division, Ext. 5545

LAWRENCE RADIATION LABORATORY
UNIVERSITY of CALIFORNIA BERKELEY

cy. 2

UCRL-19059

DISCLAIMER

This document was prepared as an account of work sponsored by the United States Government. While this document is believed to contain correct information, neither the United States Government nor any agency thereof, nor the Regents of the University of California, nor any of their employees, makes any warranty, express or implied, or assumes any legal responsibility for the accuracy, completeness, or usefulness of any information, apparatus, product, or process disclosed, or represents that its use would not infringe privately owned rights. Reference herein to any specific commercial product, process, or service by its trade name, trademark, manufacturer, or otherwise, does not necessarily constitute or imply its endorsement, recommendation, or favoring by the United States Government or any agency thereof, or the Regents of the University of California. The views and opinions of authors expressed herein do not necessarily state or reflect those of the United States Government or any agency thereof or the Regents of the University of California.

Contents

Abstract v

I. Introduction. 1

II. Experimental Apparatus. 8

A. Lasers. 8

B. Synchronization of Pulses. 16

C. Operation of the Laser at the R_2 Transition. 26

D. Normalization by Sum-Frequency Generation. 33

E. Complete Experimental Set-Up. 35

III. Theoretical Apparatus. 38

IV. Results of Experiments and Compairson with Theory. 57

A. Summary of Experimental Results. 57

B. Comparison with Theory. 65

C. Discussion. 77

Acknowledgments. 81

References. 82

FAR-INFRARED GENERATION BY NONLINEAR OPTICAL INTERACTION

Dillard Wayne Faries

Department of Physics, University of California
and
Inorganic Materials Research Division,
Lawrence Radiation Laboratory,
Berkeley, California 94720

ABSTRACT

Tunable narrow-band far-infrared generation by nonlinear optical mixing is achieved for the first time. Two ruby lasers, simultaneously Q-switched by a single rotating prism, and operated at different temperatures are used as primary sources. The laser beams, with typical peak power of one megawatt in an area of 0.2 cm^2, a divergence half-angle of 1 to 2 mrad, and a pulse duration of 30 to 50 nsec, are combined and mixed in a nonlinear crystal, primarily lithium niobate ($LiNbO_3$). The nonlinear polarization at the difference frequency induced in the crystal acts as a source for generating far-infrared. Tunability from 1.2 cm^{-1} to 8.1 cm^{-1} and from 21 cm^{-1} to 37 cm^{-1} is achieved by varying the lasing temperature and selective Q-switching of either R_1 or R_2 transitions. The output power is increased by phase-matching. Peak powers up to about 20 milliwatts are achieved. Variation of power with deviation from phase-matching is measured. The far-infrared radiation is analyzed with a far-infrared Fabry-Perot interferometer, yielding values consistent with the difference of the two ruby laser frequencies. Calculations for the power output including effects of laser mode-structure, absorption, birefringence, boundary conditions and phase-matching are presented and compared with experimental results.

I. INTRODUCTION

The motivation for difference frequency generation of electromagnetic radiation in the far-infrared region is twofold. Firstly, it offers the possibility of providing a useful source of radiation for spectroscopy in the far-infrared. Secondly, the nonlinear far infrared difference frequency generation has only been sparingly studied and needs to be placed on a firm foundation both experimentally and theoretically. The common motivation involved is a more complete understanding of the nonlinear interaction of electromagnetic radiation with matter and thus a better understanding of the nonlinear optical properties of matter.

We will be primarily concerned with the nonlinear optical process of difference frequency generation itself. This involves interaction of three electromagnetic waves in a crystal, two high frequency waves (in our case, visible light) and one far infrared wave at the difference frequency of the two visible sources. This is closely related to other nonlinear processes[1,2] (electro-optic effect, sum-frequency generation, parametric processes) which have been studied much more extensively. In principle, the study of difference frequency generation should yield information about the nonlinear material at energy levels corresponding to both the high frequency and low frequency waves. In practice, spectroscopic measurements using only one frequency can often yield more information more easily. (The information obtained by the two different methods is generally not redundant because different selection rules apply to the two cases.) Thus, in the long run, the use of difference frequency sources for spectroscopic sources may be the stronger motivation. However, we will spend very little time on

this aspect.

"Exploratory spectroscopic studies in the region between 0.05 and 3 mm in wavelength [3 to 200 cm^{-1} in wave number] began more than 50 years ago but progress has been greatly impeded by the lack of suitable bright sources so that the spectroscopy here has lagged well behind that in other parts of the spectrum."[3] There is certainly no lack of transitions in this region of the spectrum: magnetic levels (e.g. cyclotron resonance of electrons with small effective mass), phonons, vibrational levels of larger molecules, rotational levels of small molecules, crystal field splittings, energy gaps in superconductors, etc. The primary sources, mainly used in other regions of the spectrum, are not entirely satisfactory when extended into the far-infrared. Electron beam devices such as the klystron, magnetron, etc., are useful for low frequencies. Their efficiency falls off rapidly with increasing frequency. With considerable trouble, electron beam devices have been able to extend to 25 cm^{-1}. By using harmonic generation (multiples of the fundamental frequency), one can obtain higher frequencies with resultant great loss of efficiency. An additional disadvantage is the limited tunability of the frequency ($\approx \pm 5\%$). On the other hand, hot-body sources are useful for high frequencies. They produce broadband radiation, whose power spectrum falls off rapidly with decreasing frequency. For example, a perfect black body of surface area 1 cm^2 and temperature of 5000°K will do quite nicely for lighting a room, radiating approximately 1000 watts of radiation, much of which is visible, but it delivers only about 1 milliwatt in the entire range from 0 to 50 cm^{-1} into a solid angle of 2π. By contrast, difference

frequency generation is capable of producing peak powers of milliwatts in a smaller solid angle with frequency bandwidth on the order of 0.01 cm^{-1}. Thus, we can see some of the potential of this method. Let us turn now to a brief introduction to the nonlinear process.

It is usually assumed that away from resonance, the polarization $\vec{P}$ is linearly proportional to the applied electric field $\vec{E}$: $\vec{P} = \chi\vec{E}$ where χ is, in general, a tensor. One would not expect the linearity to be good at all field strengths, particularly as $\vec{E}$ becomes non-negligible compared with the atomic electric fields. Thus, one should expect an expansion in higher powers of $\vec{E}$ should be appropriate. The first-order nonlinear term implies frequency mixing because a product of two different frequency components yields frequencies which are linear combinations of the applied frequencies, namely sum and difference. Quantum mechanically speaking, difference frequency generation means a loss of a high frequency photon and a gain of a slightly lower frequency photon with the creation of a difference frequency photon. In particular, let us consider two discrete frequency components in plane-wave form

$$\vec{E}_i(\vec{r},t) = 1/2\ [\vec{\mathcal{E}}_i \exp(ik_i z - i\omega_i t) + c.c.], i = 1,2. \qquad (1)$$

This will result in a polarization of frequency $\omega_1 - \omega_2$

$$\vec{P}^{NLS}(\omega_1 - \omega_2) = 1/2 \left[\chi_D^{(2)} \vec{\mathcal{E}}_1 \vec{\mathcal{E}}_2^{\,*} \exp[i(k_1 - k_2)z - i(\omega_1 - \omega_2)t] + c.c.\right] \qquad (2)$$

and a polarization of frequency $\omega_1 + \omega_2$

$$\vec{P}^{NLS}(\omega_1 + \omega_2) = 1/2 \left[\chi_s^{(2)} \vec{\mathcal{E}}_1 \vec{\mathcal{E}}_2 \exp[i(k_1 + k_2)z - i(\omega_1 + \omega_2)t] + c.c.\right] \qquad (3)$$

We expect such polarization waves to create new fields at the new frequencies. In particular, if $\omega_1 = \omega_2$, we get the second harmonics,[4] and the dc fields.[5] Higher-order nonlinear terms will, in general, give any linear combination (with integral coefficients) of frequencies involved, e.g. $3\omega_1 - 2\omega_2$. These terms are much smaller and can usually be ignored.

Consider now only the difference frequency generation. We may note from Eq. (2) that the wave-vector and thus the phase of the polarization wave at $\omega_1 - \omega_2$ is determined by the wave-vectors of light at ω_1 and ω_2. On the other hand, the wave-vector of the propagating radiation at the difference frequency is determined by the index of refraction of the medium at frequency $\omega_1 - \omega_2$. These two wave-vectors at $\omega_1 - \omega_2$ will, in general, be different because of dispersion. The result is that the polarization wave and the radiation will be alternately in phase and out of phase as they propagate through the medium. This results in an oscillatory behavior of the power generated as a function of the thickness of the generating medium. If $\omega_1 - \omega_2 = \omega$ and $k = \frac{\omega}{c} n(\omega)$, then we may define a momentum mismatch, $\Delta\vec{k} = \vec{k}_1 - \vec{k}_2 - \vec{k}$. By using the birefringence of a crystal to compensate for the dispersion,[6,7] we can make $\Delta k = 0$, a worthwhile accomplishment as we shall soon see.

Assuming a monochromatic wave in a non-magnetic ($\mu = 1$) current-free medium, Maxwell's equations easily reduce to the wave equation

$$\vec{\nabla} \times \vec{\nabla} \times \vec{E} - \frac{\omega^2}{c^2} \vec{D} = 0. \qquad (4)$$

The displacement vector $\vec{D}$ is given by

$$\vec{D} = \vec{E} + 4\pi\vec{P}^{L} + 4\pi\vec{P}^{NL} = \varepsilon\vec{E} + 4\pi\vec{P}^{NLS}$$

where $\vec{P}^{L}$ and $\vec{P}^{NL}$ are linear and nonlinear polarizabilities, respectively, and $\vec{P}^{NLS}$ is given by Eq. (2), with $\vec{P}^{L}$ being swept into the $\varepsilon\vec{E}$ term and any local field corrections being swept into the susceptibilities ε and $\chi_D^{(2)}$. (see Ref. 1, p. 68-69) Let us make the following non-essential but simplifying assumptions: (1) infinite plane waves propagating in the z-direction, $\vec{E}(\vec{r}) = 1/2(\vec{\mathcal{E}}(z)e^{ikz} + c.c.)$; (2) $\vec{\nabla}\cdot\vec{\mathcal{E}} = 0$; (3) $\frac{1}{k}\frac{\partial^2\mathcal{E}}{\partial z^2} << \frac{\partial\mathcal{E}}{\partial z}$; (4) $\mathcal{E}(0) = 0$; (5) nonlinear medium of length ℓ with no discontinuity in ε, i.e., no reflections at boundaries; (6) ε is a scalar; (7) k is real, i.e., no absorption; and (8) the beams producing the nonlinear polarization are not depleted, thus leaving P^{NLS} with no z-dependence other than phase. Assumption (3) means physically that the rate of growth of the amplitude $\mathcal{E}$ with z does not change drastically within a wavelength. All of these assumptions give us a simplified case for estimating the generated power as a function of input powers, frequency, momentum mismatch, and length of crystal. From assumptions (1) and (2), Eq. (4) can be immediately transformed to

$$-\frac{\partial^2}{\partial z^2}\vec{E} - \frac{\varepsilon\omega^2}{c^2}\vec{E} = \frac{4\pi\omega^2}{c^2}\vec{P}^{NLS} \tag{4a}$$

which is a wave equation with the nonlinear polarization wave acting as a driving force. Making the substitutions and using assumption (3), we immediately obtain

$$-2ik\frac{\partial\vec{\mathcal{E}}}{\partial z} = \frac{4\pi\omega^2}{c^2}\vec{\vec{\chi}}_D^{(2)} : \vec{\mathcal{E}}_1\vec{\mathcal{E}}_2^{*}\exp(i\Delta kz). \tag{4b}$$

Upon integration and squaring the absolute value, we obtain the power output to be proportional to

$$|\mathcal{E}|^2 = \mathcal{E}\mathcal{E}^* = \left(\frac{2\pi\omega^2}{kC^2}\right)^2 |\chi_D^{(2)}|^2 \, |\mathcal{E}_1|^2 \, |\mathcal{E}_2|^2 \, \ell^2 \, \frac{\sin^2\left(\frac{\Delta k \ell}{2}\right)}{\left(\frac{\Delta k \ell}{2}\right)^2}. \qquad (5)$$

Thus we get power output proportional to (1) the square of the frequency, (2) the product of the power of two input sources, (3) the square of a nonlinear susceptibility and (4) the square of the length of the nonlinear medium, provided $\Delta k = 0$. For $\Delta k \, \ell \gtrsim 2\pi$, the power output is down considerably. The case of $\Delta k \neq 0$ shows the oscillatory behavior mentioned earlier.

The implications are clear. The dependence on the power of the input sources, coupled with the size of the nonlinear susceptibilities, implies a requirement of high power not satisfied until the advent of the laser. The frequency dependence, aided considerably by the fact that high frequency photons carry more energy and are thus more easily detected, means that high-frequency production, e.g., sum frequencies or large difference frequencies, is a much easier task. On the very low frequency end, detection is again very good where one can use waveguides and rectifiers. Thus the difference frequency generation at 3 GHz, the frequency separation of two axial modes of a ruby laser, was seen quite early[8] as was the visible difference frequency between the ruby laser and the 3115 A° line of a mercury discharge.[9] In spite of the difficulties, the far-infrared region is very enticing because tuning the high frequency inputs by a relatively small amount, such as could be obtained by temperature-tuning the ruby laser, would result in a far-infrared source with large tunability[10].

Several groups have reported fixed frequency far-infrared radiation by difference frequency generation. Zernike and Berman[11] detected radiation near 100 cm^{-1} resulting from the mixing of an unknown number of modes from a single pulsed neodymium glass laser. Yajima and Inoue[12] used the R_1 and R_2 lines of a single ruby laser to generate a fixed frequency, $\bar{\nu}$ = 29 cm^{-1}. Zernike[13] and Van Tran and Patel[14] have used the 9.6μ and 10.6μ CO_2 laser transitions to produce radiation in the 100 cm^{-1} range. We have used two simultaneously Q-switched ruby lasers, tuned both by temperature and to the different R-lines, to produce tunable, narrow band radiation from 1.2 cm^{-1} to 8.1 cm^{-1} and from 21 cm^{-1} to 37 cm^{-1}. This is but a small step in what promises to be a very fruitful area of research.

II. EXPERIMENTAL APPARATUS

Lasers

The lasers used are fairly typical ruby lasers. The cylindrical ruby rods (0.05% Cr^{+3}) have end faces cut parallel within 2 seconds of arc and flat to $\lambda/10$. One rod is $3\frac{1}{4}$ inches long and has a diameter of $\frac{1}{4}$ inch; the other is 4 inches long with a diameter of $\frac{3}{8}$ inch. The fact that we used two different sizes is an accident of history and not a purposeful, calculated move. The rod in each case is surrounded by a cylindrical glass shield through which fluid is circulated to maintain the ruby at a fixed temperature. Around the glass shield is a helical xenon flash lamp through which a capacitor bank is discharged to produce a pumping light which pumps the Cr^{+3} ions into an excited metastable state within a few milliseconds. (See Fig. 1 for an energy diagram of Cr^{+3} in ruby.) The energy discharged through the lamps varies from about 500 joules to about 2000 joules. The flash lamps are cooled only by contact with the air and a slow flow of nitrogen gas (approximately 4 cubic feet per minute). Thus the lamps are not flashed too frequently, generally once every five minutes. The lamps are housed in a cylindrical reflector with polished silver surface, but this was found to be non-critical. Diffuse surfaces make little change in the threshold pumping power required for lasing. Electrical connections to the flash lamp are made with flexible leads to reduce mechanical vibrations transmitted from the lamp to the rest of the system.

In order to produce two different frequencies with the two lasers,

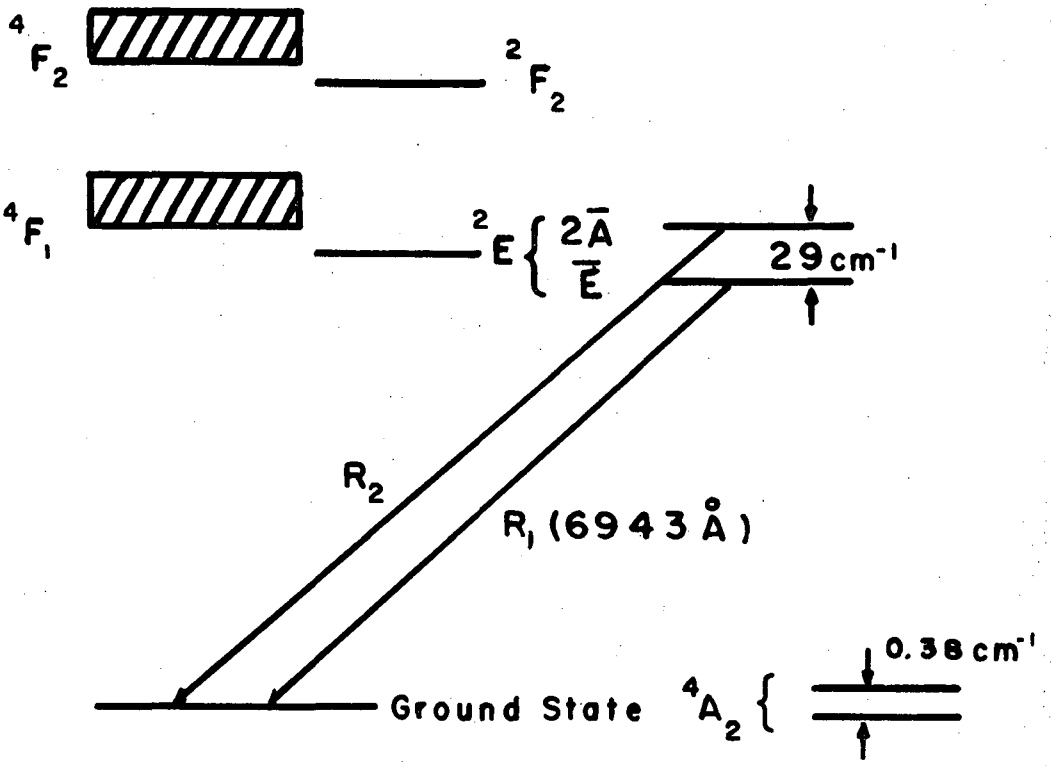

XBL 698-1117

Fig. 1 Energy level Diagram of Cr^{+3} in Ruby. There is a fast radiationless transition from the F levels to the metastable state ^2E (lifetime of 3 msec). Thus the ^2E levels become more populated than the ground state levels through optical pumping on the F levels.

we operate the two lasers at different temperatures,[16,17] either both lasing on the R_1 transition or one on the R_1 transition and the other on the R_2 transition (Fig. 1). A wide range of temperature tuning is required for a wide range of frequency tuning. Above room temperature, the linewidth broadens rapidly with temperature increase,[17] the gain thus decreases and laser action is impractical. At liquid nitrogen temperature, the gain gets very large. To prevent spontaneous lasing action from extraneous surfaces, the rods must be cut at the Brewster angle and a mechanism for Q-switching other than the rotating prism is required. However, the rotating prism is necessary for our synchronization scheme (see the section on synchronization of pulses). If we were able to use one laser from room temperature down to 77°K, this would represent a range of difference frequencies, $|\bar{\nu}$ (Room temperature) - $\bar{\nu}$ (cooled)$|$, from 0 to 18 cm^{-1}. This might be possible to achieve with more versatile means of synchronizing the pulses such as Kerr or Pockels cell Q-switching.

As the next best thing, we attempted to use dry nitrogen gas, cooled in heat-exchange coils by liquid nitrogen. This was capable of cooling the ruby to about -100°C. There were, however, large temperature gradients along the rod, causing a very erratic behavior of the laser. We were thus forced to go to coolants with more heat capacity, namely, liquids. Several liquids were tried and rejected for a variety of reasons such as reaction on O-rings or plumbing hoses, fear of low flash points, and insufficiently low freezing point. One failure worth mentioning is the use of silicone oils. It is not easily learned, without possibly catastrophic experience, that a reaction occurs under

high-intensity lamps, leaving a brown precipitate and releasing gas. It is also difficult to remove from cracks, does not evaporate, and may come back to haunt a laser many weeks after its intended banishment. Ethyl alcohol, on the other hand, keeps the laser quite happy.

The temperature control system consists of a bath of approximately one gallon of fluid, a thermoregulator to switch a heater on or off, and a pump to circulate the liquid through the laser. The thermoregulators are good for control to ±0.01°C. The problem of overshooting the desired temperature and the problem of circulation make control no better than ±0.1°C. In order to avoid overshoot, the heating and cooling must be closely balanced. In the room-temperature control, tap water cools the bath via coils in the water. For the cooled laser, the ethyl alcohol is cooled by flowing through copper walls of a bucket of dry ice. This is capable of cooling the laser below -50°C, but regulation is not good below -40°C. With a temperature coefficient of 0.135 $cm^{-1}/°K$,[16] this gives us a tuning range of over 8 cm^{-1}.

To complete the laser, an optical cavity is required, two mirrors providing feedback to the amplifying medium, ruby, to provide oscillation (see Fig. 2). The oscillation condition is that a round trip through the cavity yields gain 1, i.e., $r_1 r_2 e^{2g\ell} = 1$ where r_1 and r_2 are the reflectivities of the mirrors, ℓ is the length of the ruby rod, and g is the gain per unit length. Generally one mirror's reflectivity is high, the other being lower, maintaining the laser oscillation condition but allowing as much power as possible to leave the cavity and be used. The high reflectivity mirror is discussed later, being determined by considerations of power and timing.

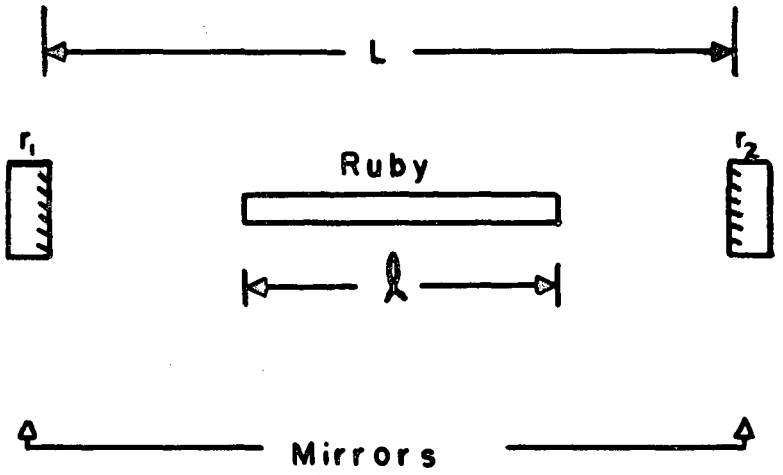

XBL 698-1118

Fig. 2 Simple Laser Cavity. r_1 and r_2 are the reflectivity of the mirrors.

Special considerations for producing the R_2- line are also discussed later. We will now consider the low reflectivity or output mirror.

The cavity formed by the two mirrors essentially forms a Fabry-Perot interferometer, which will support standing wave oscillations separated in wave number by $^1/2L$, called the free spectral range of a Fabry-Perot interferometer. L is typically 50 cm, making $\Delta\bar{\nu} \sim 0.01$ cm^{-1}. Since the fluorescence linewidth of the R-transitions in ruby is 5 - 10 cm^{-1}[17] at room temperature, we should expect many lines to lase and give a broad frequency band, i.e., on the order of a few wavenumbers broad. This is illustrated in the Fabry-Perot interferogram of the laser output of Fig. 3a. With a spacing of 0.25 cm between the plates of the Fabry-Perot, this shows the output to be about 1 cm^{-1} in breadth. One would like to make the frequency band as narrow as possible, increasing the power per unit frequency width. This is possible by the use of a resonant reflector as the output mirror.[18-21] This consists of two glass optical flats aligned parallel with a spacing of 2.5 cm. Each set of two surfaces form a low reflectivity Fabry-Perot interferometer used in reflection. The coupling makes the analysis non-trivial,[18] but basically there are maximum reflection coefficients spaced in wavenumbers by $\frac{1}{2d}$, the free spectral range for a given pair of surfaces. The longer spacings in the reflector are about 2.5 cm, yielding a free spectral range of 0.2 cm^{-1}. The shorter spacings, the thickness of the flats, yield a free spectral range on the order of 1 cm^{-1}, thus modulating the reflectivity vs. wavenumber with this period. This leaves a few modes, spaced by 0.2 cm^{-1}, with higher reflectivity at the output mirror and situated near the peak of the fluorescence line, which

Fig. 3 Fabry-Perot Interferograms of Laser Output. (a) Output at low resolution (free spectral range of 2 cm^{-1}). (b), (c), (d) Output with a resonant reflector in the laser cavity at low resolution (b) and at high resolution [(c), (d)] (free spectral range of 0.5 cm^{-1}). The laser beam is diffusely scattered by a ground glass before the interferometer. The pictures are obtained by placing a camera, focused at infinity, directly after the interferometer. Smaller spacings of the Fabry-Perot plates give a larger free spectral range , less resolution, and a set of rings of larger radii [Fig. (a), (b)]. If the source has spectral content narrower than the instrumental linewidth of the interferometer, a set of narrow rings appears [Fig. (b)]. Fig. (a) shows a spectral content of many lines, not completely resolved, with a total width of approximately half the free spectral range of 2 cm^{-1}. Fig. (c) and (d) each show two frequency modes separated by 0.2 cm^{-1}. In Fig. (c), one mode is dominant; Fig. (d) shows modes of nearly equal intensity.

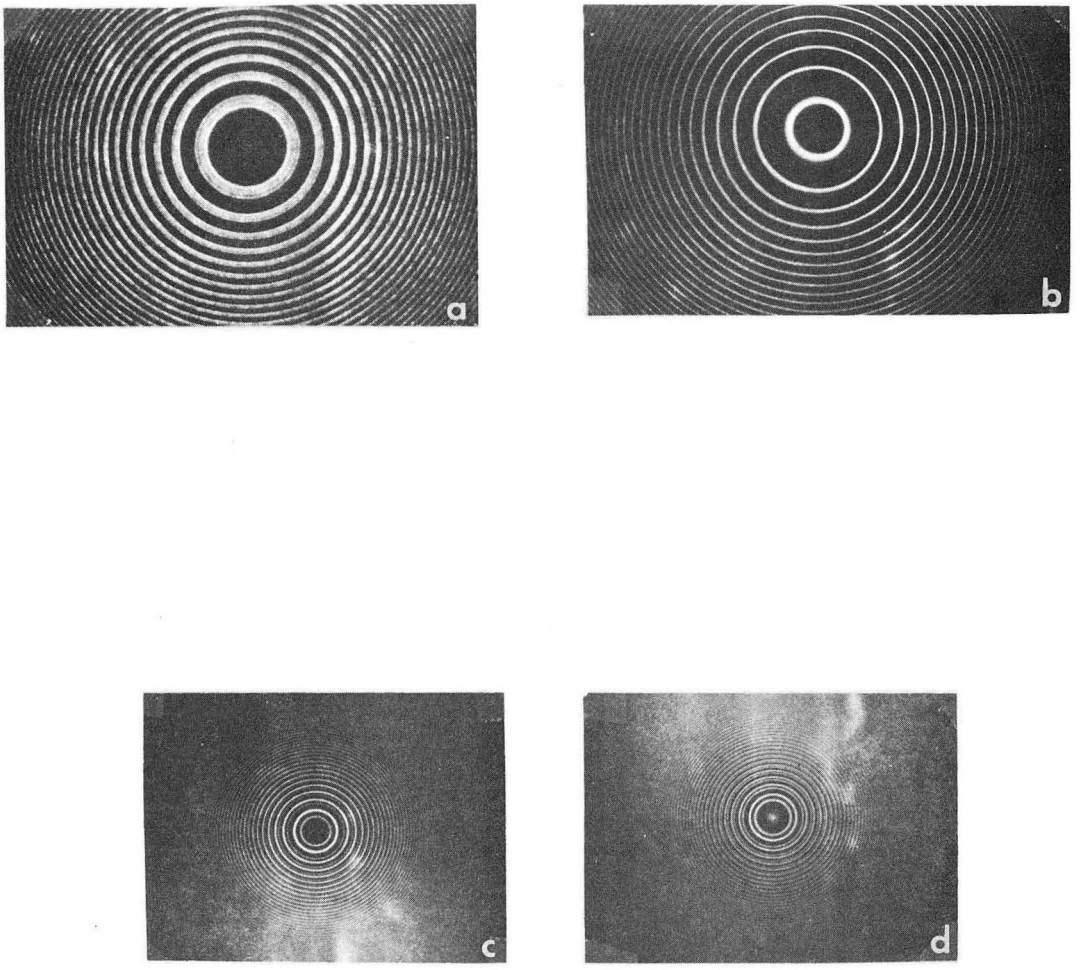

XBB 697-4902-A

Fig. 3

are favored to satisfy the oscillation condition. Thus the laser generally lases in one or two of these modes, illustrated by interferograms of the outputs shown in Fig. 3.

Synchronization of Pulses

The simple cavity in the above discussion is unsatisfactory for the following reason: The energy comes out in a long irregular train of pulses, with a total pulse length of the order of a millisecond. It would be useful not only to compress the energy in the frequency domain but also in the time domain. One should like to hold back the energy stored in the Cr^{+3} ions until the gain is large and all the energy will be dumped into a short pulse, with duration on the order of tens of nanoseconds. There are several well-established methods[22] of doing this, so-called Q-switching methods: Oscillation is prevented by lowering the Q of the cavity, (lowering feedback or introducing losses). At a time when the gain is large, the Q is "switched" to a higher value and oscillations are allowed. The most common methods are saturable absorbers, dyes placed in the cavity to provide loss until the absorption saturates, rotating reflectors, providing feedback only for the short time in which they are aligned properly, and Kerr or Pockels cells acting as fast electronic shutters.

Now we add a complication. Not only do we want to produce Q-switched pulses, but we want to produce them in two separate lasers at the same time. To synchronize the millisecond non-Q-switched pulses is not difficult[23]: Simply starting the flash lamps from a common pulse would generally suffice. The Q-switched case is more difficult.

Two methods using saturable dyes are of historical interest.

Soffer and McFarland[24] used one Q-switched laser to "burn a hole" (saturate) the absorption) in a saturable dye of another laser cavity. This resulted in a delayed "synchronized" pulse, delays being consistently on the order of 100 nanosecond. Gregg and Thomas[25] achieved tremendous synchronization (± 3 nsec) of five lasers by interlocking the cavities, using each of several saturable absorber cells in more than one cavity. As useful as this technique was for increasing power for production of plasmas, it is useless for our problem because the frequencies locked together as well as the timing. Thus one did not have two <u>independent</u> lasers at the same time. A rather specialized technique was used by Van Tran and Kehl[26] to Q-switch a neodymium and a ruby laser together. A beam splitter with high reflectivity at the ruby frequency and high transmissivity at the neodymium frequency was used to combine the two cavities, Q-switching both cavities with a single rotating prism. This was quite effective but was limited to special cases where the frequency difference of the two lasers is quite large.

The following property of the roof-top prism allows us, in principle, to Q-switch any number of lasers independently from a single rotating prism, changing the temperature, relative timing, direction, or laser material at will. Any ray entering the broad face in the plane perpendicular to the roof edge is reflected back parallel to itself. (Total reflection occurs over a small range of angles.) The independent optical paths of two lasers are both centered at the roof edge, but at an angle to each other [Fig. 4]. The prism is rotated about a horizontal axis, with its roof edge perpendicular to the axis of rotation. With a laser pumped, Q-switching begins when the roof edge of the rotating prism

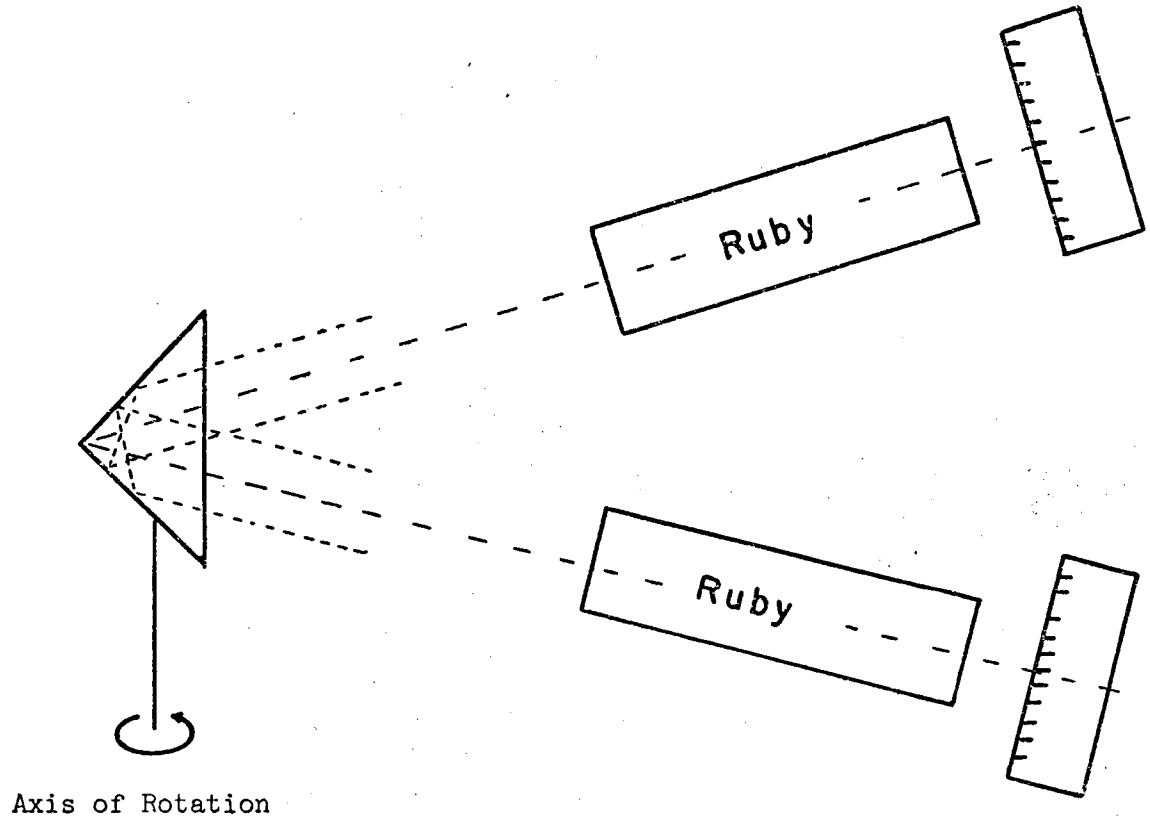

Fig. 4 Top view of two lasers Q-switched from the same rotating prism. The prism reflects an incoming ray back parallel to itself.

reaches the position perpendicular to the optical path of the laser. Therefore the relative timing of the two lasers can be controlled by slight tilting of the optical path of one laser with respect to the horizontal plane [Fig. 5]. If the cavity is bent using prisms [see Fig. 10b], the timing can be controlled by tilting a prism [P_2] without changing the direction of the laser output. A rotation rate of 400 cps and a screw with 80 threads/inch on a lever arm of 12 inches makes a fine tuning of a few nanoseconds possible.

Upon trying the synchronization, we find a jitter, an inconsistency in relative timing, of as much as 50 nsec. With pulses of approximately 30-50 nsec pulse length, this is not a hopeless situation, but it is discouraging. Let us consider the variables involved and their possible effects and remedies. The possible causes of jitter are: (1) mechanical vibration, (2) variations in the temperature of the ruby rods, (3) variations in the timing of the initiation of the flash, (4) variations in voltage applied to flash lamps, (5) variations of pumping power of the flash lamps due to other reasons.

We have taken several precautions against mechanical vibrations. The rotating prism is mounted on a separate steel and concrete column, with rubber mounts to absorb vibrations. The laser tables are mounted on a 1-inch thick steel plate on a heavy wooden table. As mentioned before, the flash lamps are connected with flexible leads to avoid

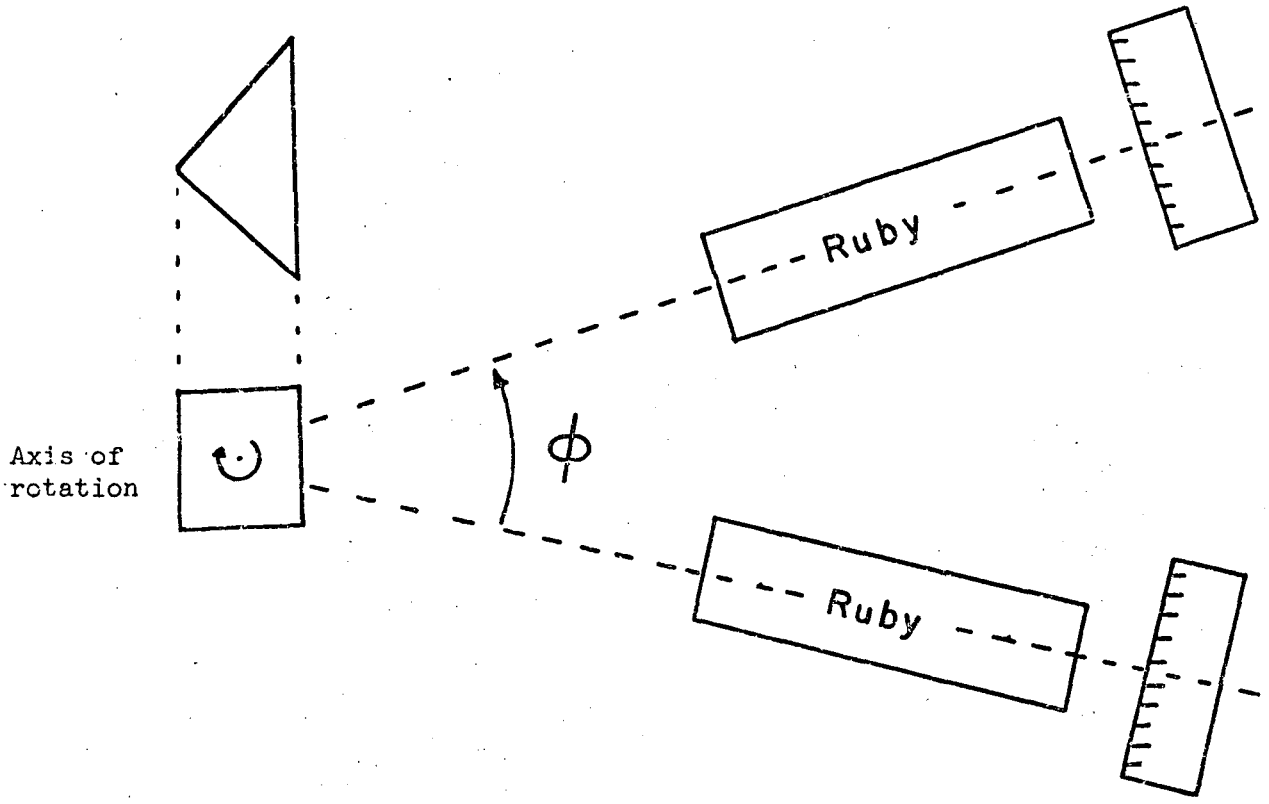

Fig. 5 Side view of two lasers Q-switched from the same rotating prism. ϕ is the projected angle in the plane of the paper. ϕ controls the relative timing of the two lasers; it is greatly exaggerated here.

shaking the table upon flashing. While the other variables might be expected to vary their effect according to the threshold and how close to threshold one is working, mechanical vibrations should be more consistent, provided no changes are made in the mechanical system. Since the jitter varies greatly, sometimes small and sometimes large, mechanical vibration apparently has a small effect.

Variations in the temperature of the ruby rod can be made easily to check its effect. We can control the temperature to ± 0.1°C. Fig. 6 shows a series of pictures with a change of temperature of 1.2°C for one of the lasers. Tens of degrees are required to move the relative timing 100 nsec. Thus we seem to be on the safe side here.

The initiation of the flash requires an explanation. A diode and a small light are placed near the rotating prism at a given point on a circle around the axis of rotation. When the prism faces the light, it reflects the light into the diode, giving a pulse, marking the time when the prism passes this point. The pulse is amplified, fed into a Del-a-Gate (LRL Counting Equipment) which produces a sharp 6 volt pulse used to initiate the flash. The time of initiation before the prism aligns with the laser cavities can be varied by moving the light and diode around the axis of rotation. The pulses from the Del-a-Gate come every 2.5 msec and are found to have a jitter of 5 μsec. This appears to be caused by electronic pickup and could probably be eliminated. However, Fig. 7a shows the size of the effect. A change of 100 μsec results in a 50 nsec change in laser timing. Thus a jitter of 5 μsec in the length of the millisecond flash before Q-switching should result in only a few nanoseconds of jitter.

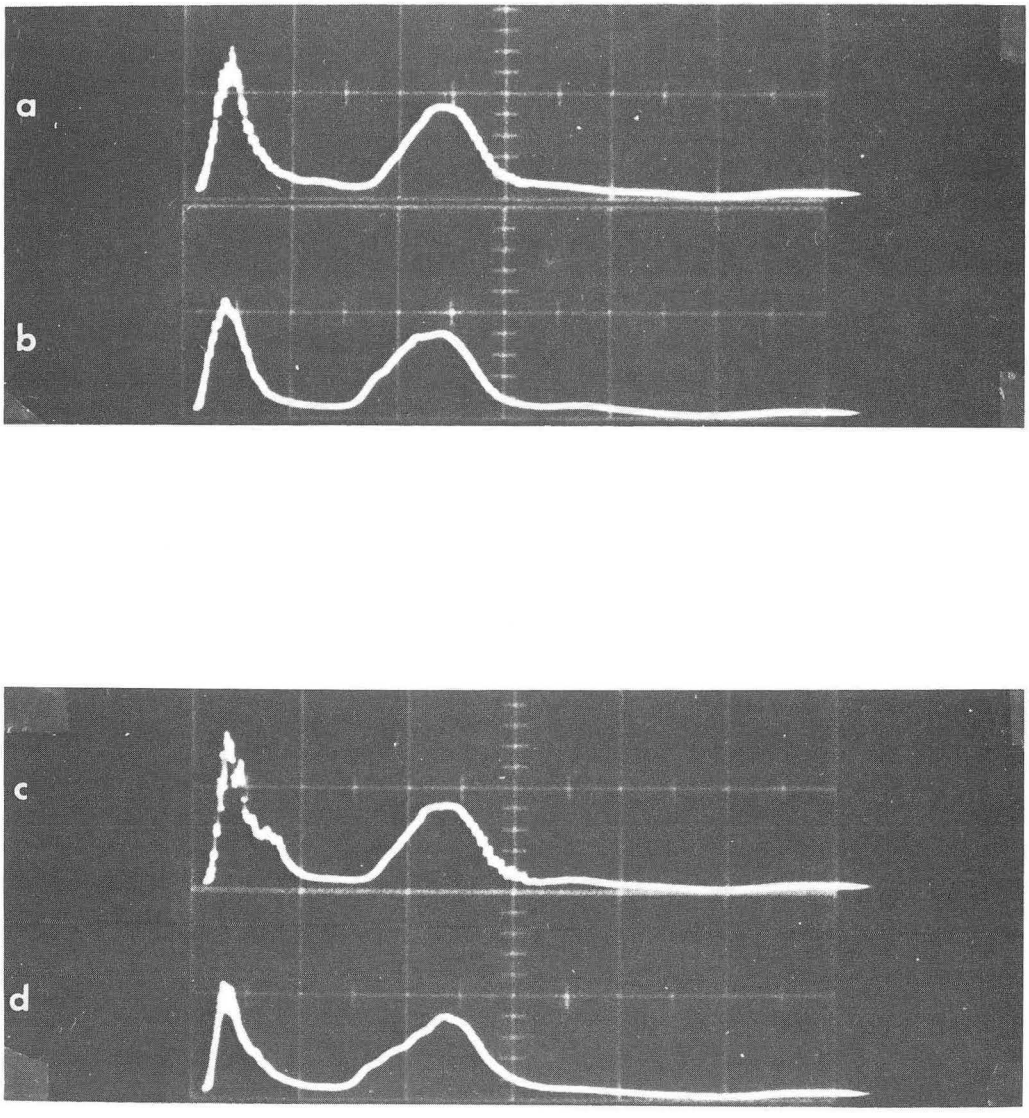

XBB 697-4899-A

Fig. 6 Effect of temperature on relative timing of laser pulses. The laser signals are displayed on a single oscilloscope trace at a sweep rate of 100 nsec/div, one laser signal being delayed by 125 nsec. Each photograph shows two trials. (a), (b) temperatures of the two lasers are equal. (c), (d) temperatures of the two lasers differ by 1.2°C. Relative timing is essentially unchanged.

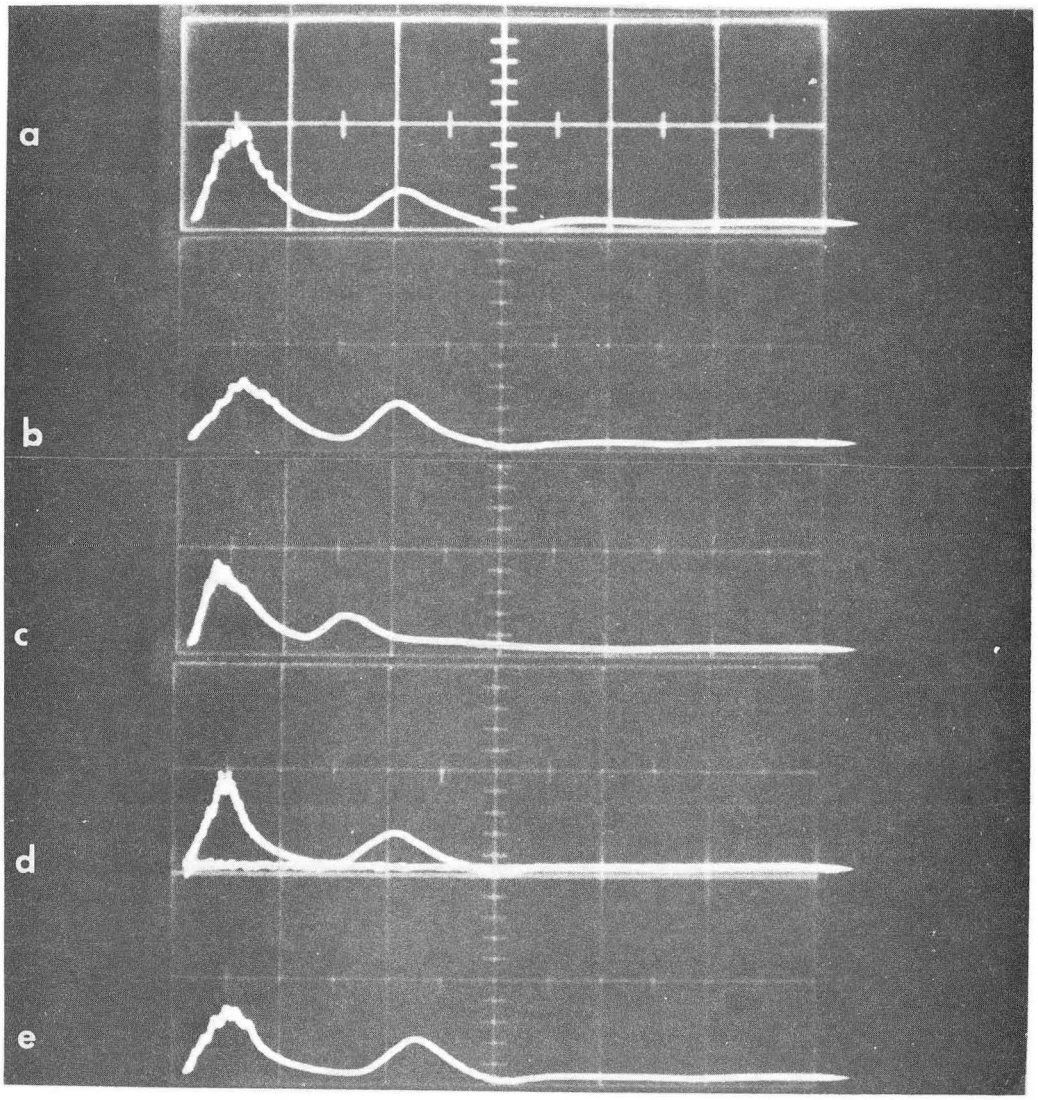

XBB 697-4900-A

Fig. 7a Effect of timing of initiation of flash on relative timing of laser pulses. The laser signals are displayed on a sing oscilloscope trace at a sweep rate of 100 nsec/div, one laser signal being delayed by 125 nsec. The interval between initiation of the flash and the Q-switched pulses is 100 μsec less for trace (c) than for all the other traces.

The voltage variation can, of course, have a strong effect near threshold; a small variation can be the difference between lasing or not lasing. Thus we must work sufficiently higher than threshold, 100 - 200 volts. In this regime a further increase of 100 volts may change the timing by 50 nsec. Since the voltage can be easily set to ± 10 volts, this represents no problem.

This seems to lay the blame on some inconsistency in the flashing of the pumping lamps. It may be simply a problem of getting them to a stationary operating temperature. The larger laser shows a strong time dependence in its power output, the first shot being strong and subsequent shots being weaker. Accompanying this, the relative timing walks off by approximately 100 or 200 nsec. (See Figure 7b) Since the lamps are different (even if they were made identical, they would generally be used at different operating conditions), it is reasonable that fluctuations will affect the timing adversely, particularly since the cooling for the lamps is quite poor. If the lamp conditions become approximately equal, then fluctuations should be small. This condition was apparently reached in using the larger laser for lasing on the R_1 line. This is because the threshold for the R_2 line in the smaller laser is more nearly equal to the R_1 line threshold in the larger laser. At worst, approximately half of the attempts at synchronization in a given run yielded considerable overlap; at best, as in the R_1 - R_2 runs, nearly all attempts were useful. Making the lasers identical and in a symmetrical set-up might improve the situation, but by nature these experiments are not symmetrical: We want different frequencies from the two lasers. A set-up with water-cooled lamps does

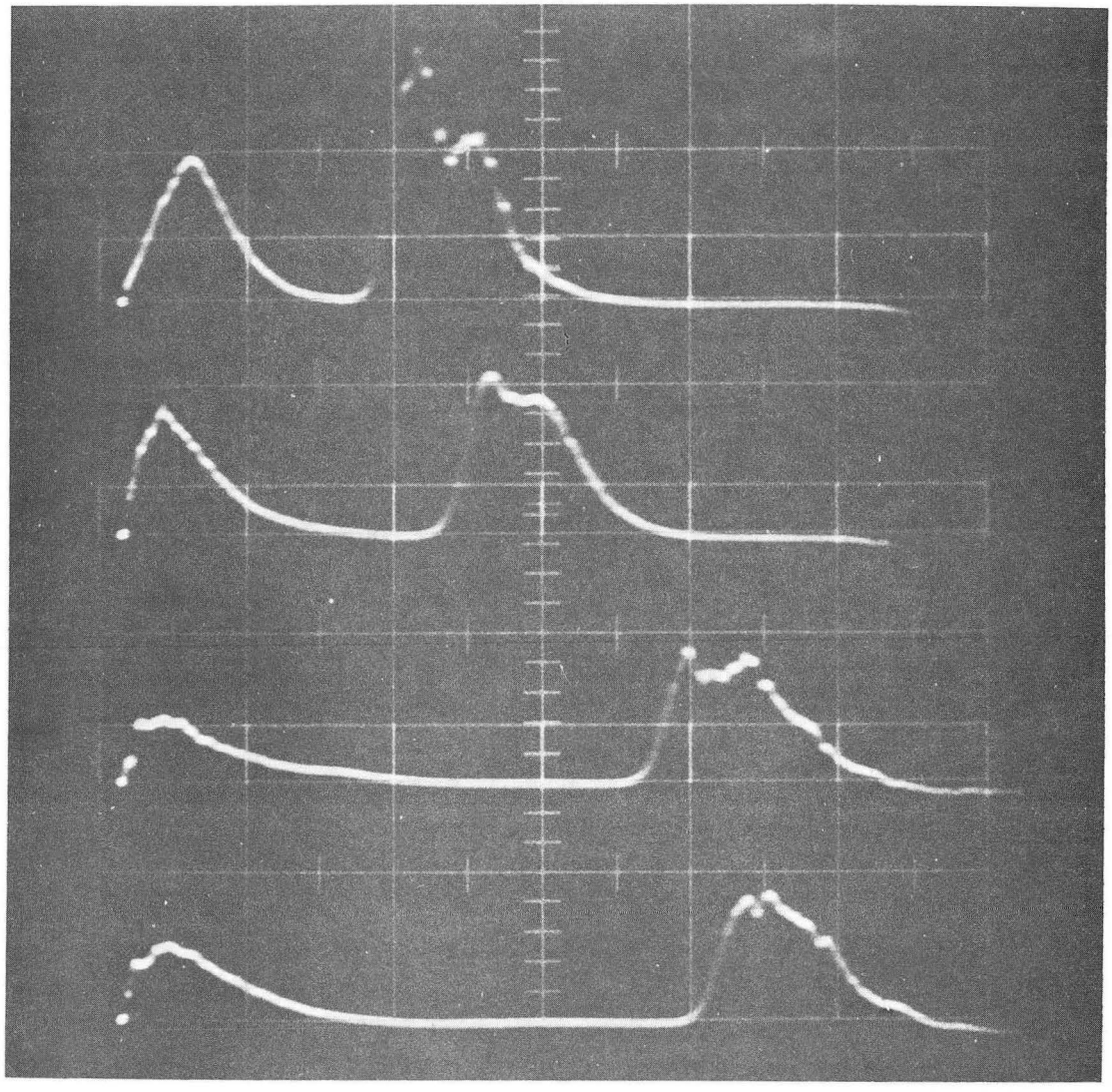

XBB 697-4901-A

Fig. 7b Change of relative timing of laser pulses with warming of flash lamps. The laser signals are displayed on a single oscilloscope trace at a sweep rate of 50 nsec/div, one laser signal being delayed by 125 nsec. Relative timing changes by more than 100 nsec as the lamps warm up from the four consecutive firings.

seem worth trying.

Operation of the Laser at the R_2 Transition

The gain factor, g, in the oscillation condition, $r_1 r_2 e^{gl} = 1$, can be written as

$$g = a(n_u - n_L) \tag{5a}$$

where a is proportional to the transition probability between the upper and lower states of the active medium and n_L, n_u are the populations of the lower and upper state, respectively. When $n_L \geqslant n_u$, then $g \leqslant 0$ and the usual z-dependence of light in the medium exp $(-|g|z)$ represents a loss. If $n_u > n_L$, then $g > 0$ and the negative absorption implies gain in the medium, exp (gz), with $g > 0$.

In the case of the ruby laser (see Fig. 1), both the $2\bar{A}$ and the $\bar{E}$ states of Cr^{+3} are populated by the flash and represent upper states while the ground states $^4A_2$ represent the lower states. Because of fast relaxation between $2\bar{A}$ and $\bar{E}$, they remain in approximate thermal equilibrium with each other, the ratios of their populations being given by a Boltzmann factor exp $(-\Delta/kT)$, where $\Delta = 29$ cm^{-1} is the energy separation between $2\bar{A}$ and $\bar{E}$. At room temperature, this means $n_{\bar{E}} \cong 1.12\, n_{2\bar{A}}$. This in itself discriminates against the R_2-transition. Thus, even if the transition probabilities for R_1 and R_2 transitions were equal, R_1 will always reach the lasing threshold first. Because of fast relaxation between the two levels, the $2\bar{A}$ level will be drained as the $\bar{E}$ level is being drained. Further discrimination occurs in the transition probabilities: $a(R_1^{\perp}) : a(R_1^{\parallel}) : a(R_2^{\perp}) : a(R_2^{\parallel}) = 10 : 2 : 7 : 4$, where $\perp$ and $\parallel$ refer to ordinary and extraordinary polarizations, respectively.[27]

The combination of the Boltzmann population ratio and the ratios above gives Fig. 8, a plot of $g(R_2^{\perp})$ versus $g(R_1^{\perp})$.[28] The equation is given in Fig. 8. Using such plots with the oscillation condition including any losses introduced, one can determine conditions, e.g. reflectivity of mirrors, length of rod, pumping power, under which R_2-oscillation will occur provided we discriminate sufficiently against R_1 by some means.

The simplest means, in principle, to discriminate against R_1 is to place a polarizer in the cavity, allowing only extraordinary polarizations (note that $a(R_2^{\parallel})$: $a(R_1^{\parallel})$ = 2:1). However, this requires very high pumping powers, requiring several times the population difference to achieve the same gain as $R_1^{\perp}$, and is thus not very convenient. Another simple means is the use of interference filters as cavity mirrors,[28] selectively reflecting R_2. This is a useful technique but limited to a narrow band of frequencies. Acquiring an interference filter capable of withstanding Q-switched laser powers and providing sufficient discrimination between the R_1 and R_2 lines over a range of temperatures is not easy.

Several people[12,29,30] have successfully used the Lyot[31] - Öhman[32] filter to produce lasing action at the R_2-transition. The filter consists of a plate of birefrigent material (in our case, quartz) between two parallel polarizers. The optic axis of the plate is perpendicular to the direction of propagation and at 45° to the polarization transmitted by the polarizers. Defining a "retardation wavelength", λ_R, by

$$\frac{1}{\lambda_R} = \frac{n_e}{\lambda_o} - \frac{n_o}{\lambda_o} \qquad (5b)$$

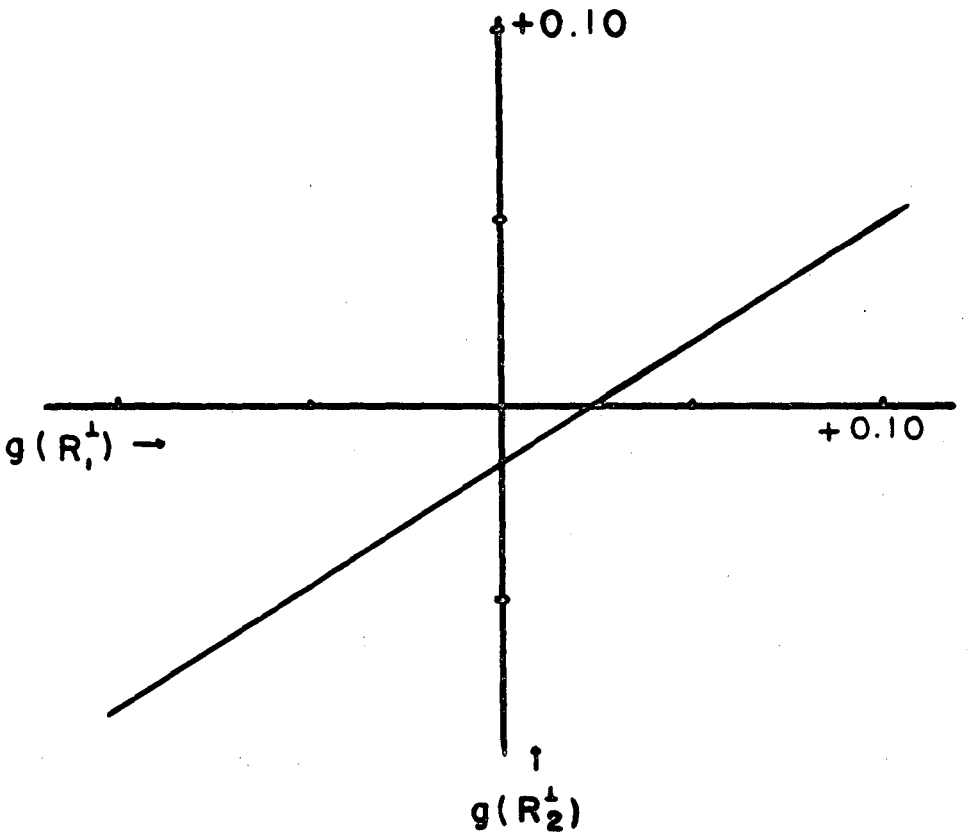

XBL 698-1121

Fig. 8 Relation between Gain of $R_2^{\perp}$ - Transition and $R_1^{\perp}$ - Transition. The equation is

$$g(R_2^{\perp}) = \frac{a(R_2^{\perp})}{a(R_1^{\perp})} \left(\frac{1 + 3\chi}{3 + \chi}\right) g(R_1^{\perp}) - \frac{a(R_2^{\perp})}{2} N \left(\frac{1 - \chi}{3 + \chi}\right)$$

where N is the density of Cr^{+3} and $\chi = \exp(-\Delta/kT)$.

where λ_o is the vacuum wavelength, n_e, n_o are the extraordinary and ordinary indices of refraction, we see that a plate thickness, d, of an integral number of "retardation wavelengths" results in no change in the polarization in passing through the quartz and thus 100% transmission through the filter. Half-integral number of λ_R means a change in the polarization by 90° and a resultant zero transmission. At intermediate thicknesses, the transmission is given by

$$T = \cos^2 \frac{\pi d}{\lambda_R} = \cos^2 \frac{\pi d}{\lambda_o} (n_e - n_o). \qquad (5c)$$

A given thickness of quartz alternately passes and stops light as one sweeps the frequency. By changing the thickness one changes the frequency difference between pass and stop bands. One should like to choose a thickness such that we get a pass band at R_2 and a stop band at R_1. The thickness specifies the distance between bands. To actually tune the pass band to R_2, one can use several methods. One can change the temperature,[29] or one can rotate the crystal.[12,30] Rotation about the c-axis increases the path length as $(\cos \theta)^{-1}$, θ being the angle of incidence. Rotation about an axis perpendicular to both the beam and the c-axis also increases the path length as $(\cos \theta)^{-1}$, but decreases the index difference as $\cos^2 \theta$; thus there is an effective decrease in crystal thickness as $\cos \theta$. $\cos \theta$ moves slowly near $\theta = 0$ so that fine tuning is easily achieved.

We use a single polarizer and a 1 cm thick quartz plate (see Fig. 9a). The light passes through the polarizer and quartz plate, is reflected and again passes through the quartz plate and the polarizer. Thus we have a complete Lyot-Öhman filter, the single polarizer serving as both

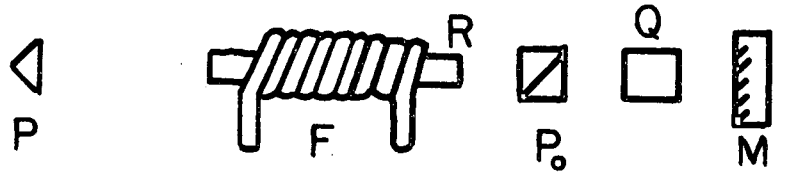

XBL 698-1122

Fig. 9a Cavity Configuration for Lasing at R_2-Transition. F = flash lamp, M = dielectric-coated mirror, P = prism, P_o = polarizer, Q = quartz, R = ruby rod.

polarizers and the 1 cm quartz plate acting as a 2 cm quartz plate because of the double traversal. We rotate the quartz crystal about the axis perpendicular to both the beam and the c-axis. In order to keep the threshold from becoming too high, a 70% dielectric-coated mirror is used as the output mirror. The threshold pumping power is about 50% higher for this situation than for R_1 - line production using the 25% resonant reflector. Theoretically, one could eliminate the polarizer. This requires that the gain for a round trip of R_2 through the cavity be larger than the gain for a round trip of R_1. With the quartz plate set properly, the polarization of the R_2-line will return from its double traversal of the quartz plate unchanged while polarization of the R_1-line will be rotated by 90°. Thus, the condition to make the R_2 transition lase before R_1 is $2g(R_2^{\perp}) > g(R_1^{\perp}) + g(R_1^{\parallel})$. This is possible theoretically since $2a(R_2^{\perp}) > a(R_1^{\perp}) + a(R_1^{\parallel})$. The relation between $g(R_2^{\perp})$ and $g(R_1)$, derived from the Boltzmann equilibrium condition $n_{2\bar{A}}/n_{\bar{E}} = \exp[\frac{-\Delta}{kT}]$, is given by

$$2g(R_2^{\perp}) = \frac{2\,a(R_2^{\perp})}{a(R_1^{\perp}) + a(R_1^{\parallel})}\left[\frac{1 + 3\exp(-\Delta/kT)}{3 + \exp(-\Delta/kT)}\right]\left[g(R_1^{\perp}) + g(R_1^{\parallel})\right] - N\,a(R_2^{\perp})\left[\frac{1 - \exp(-\Delta/kT)}{3 + \exp(-\Delta/kT)}\right] \tag{5d}$$

where N is the density of chromium ions. This equation is plotted in Fig. 9b. The condition for the R_2 line to lase first is only reached for $g(R_1^{\perp})$ greater than 0.2. Since our typical operating condition is near $g(R_1^{\perp}) = 0.1$, this requires prohibitively high pumping powers for our system.

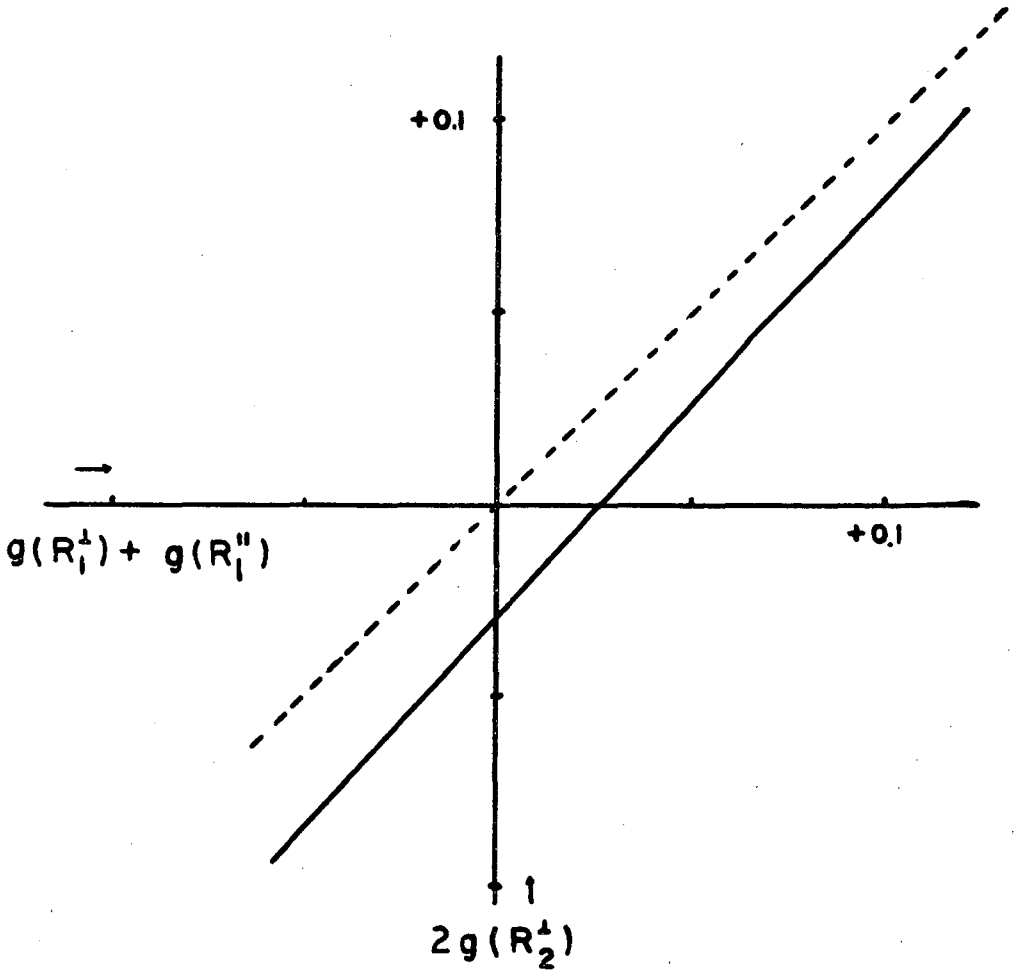

XBL 698-1123

Fig. 9b Relation of Competing Gains in Case of No Polarizer in Cavity. The dotted line describes the relation $g(R_1^{\perp}) + g(R_1^{\parallel}) = 2g(R_2^{\perp})$. The solid line describes the actual relation between $g(R_2^{\perp})$ and $g(R_1^{\perp}) + g(R_1^{\parallel})$. If $2g(R_2^{\perp}) > g(R_1^{\perp}) + g(R_1^{\parallel})$, the laser can lase on the R_2 transition without a polarizer in the cavity.

Fig. 10a shows two spectra of the laser output, one showing the R_1-line, the other showing the R_2-line. The width of the lines is due to a wide slit on the spectrograph.

Normalization by Sum-Frequency Generation

Since the synchronization may have considerable jitter and laser pulses may vary in their spatial and temporal dependence, the space-time overlap on which the total output of difference-frequency radiation depends may vary wildly from shot to shot. It is thus important to have a normalization procedure, a process to eliminate the dependence on the space-time overlap. Simultaneous detection of another nonlinear process of the same order, the sum-frequency generation, should serve the purpose. Normalization by sum-frequency generation is ideal for eliminating fluctuations in the time overlapping, which is the major difficulty in our experiments, but is not so effective for eliminating fluctuations in the space overlapping because the effects of spatial structure of laser beams on sum and difference frequency generation are different. This will become clear later, when the effect of a finite beam is treated in the theory.

Another problem appears: the second-harmonic generation of each laser frequency also occurs and must be eliminated. This problem has been solved by the techniques of Maier et al.[33] and Armstrong.[34] A nonlinear crystal of symmetry $\bar{4}2m$ or $\bar{4}3m$ (potassium dihydrogen phosphate, KDP, in our case) is cut with faces perpendicular to the 110 and mounted with the z-axis vertical, the x-y plane horizontal. From symmetry requirements the only non-zero nonlinear susceptibility coefficients χ_{ijk} $\left(P_i = \chi_{ijk} E_j E_k\right)$, are χ_{xyz}, χ_{zxy}, χ_{yzx}.[12] One laser

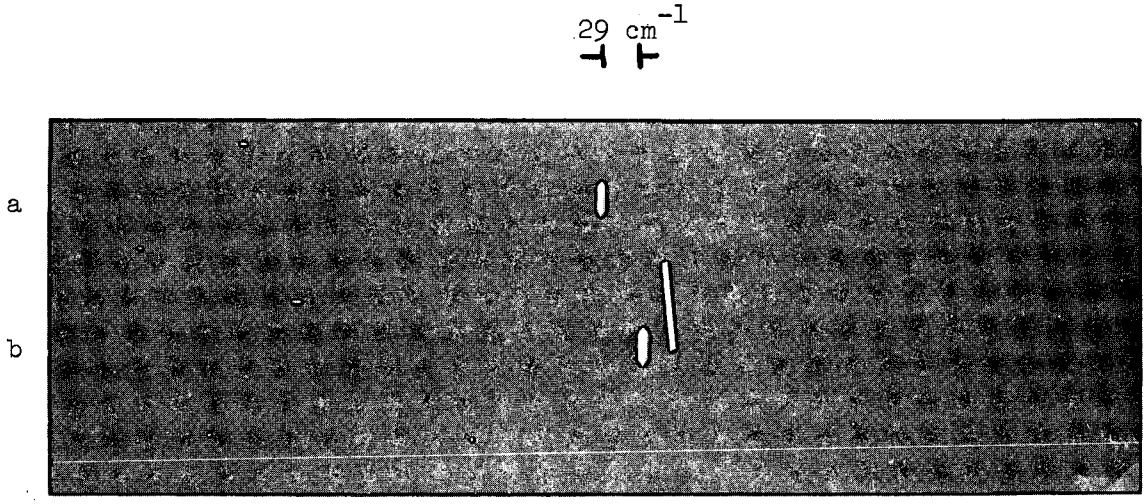

XBB 697-4903-A

Fig. 10a Laser output spectra using spectrograph. (a) lasing on R_2 transition. (b) lasing on R_1 transition. The width of the lines is due to a wide slit and overexposure.

is polarized vertically, the other horizontally. The horizontal polarization produces only P_z at the second-harmonic frequency; the vertical produces no second harmonic. Thus the second-harmonic can be eliminated by a polarizer passing only horizontal polarization. The combination of vertical and horizontal gives sum-frequency polarizations P_x and P_y. The ratio of sum-frequency to second-harmonic radiation detected can thus be made as high as 50 or 100.

Complete Experimental Set-up (see Fig. 10b)

The pulses of the two lasers are detected by two biplanar photodiodes, whose outputs are displayed on a Tektronix 519 oscilloscope. One output is delayed by a 125-nanosecond delay line to separate the displays. Typical outputs are one megawatt in an area of 0.2 cm^2, a divergence half-angle of 1.5 mrad, and a pulse duration of 30 nsec. This power is usually distributed into two frequency modes separated by 0.2 cm^{-1}. The two beams are made coincident and parallel (within one minute of arc) by careful adjustment of a prism (P_4) and the dielectric-coated beam splitter. The beam splitter is nominally 50-50, but reflects more vertical (perpendicular to the plane of incidence) polarization and transmits more horizontal (about 65%). Our lasers are polarized, one vertically, one horizontally. Thus the combined beam goes into two branches, one more powerful than the other. The higher intensity beam is made to impinge on a nonlinear crystal for difference frequency generation. The crystal is mounted on a rotatable table directly in front of a light pipe leading to a far-infrared detector. A black polyethylene filter cuts the laser radiation, passes the far-infrared. The other branch goes to the normalization scheme.

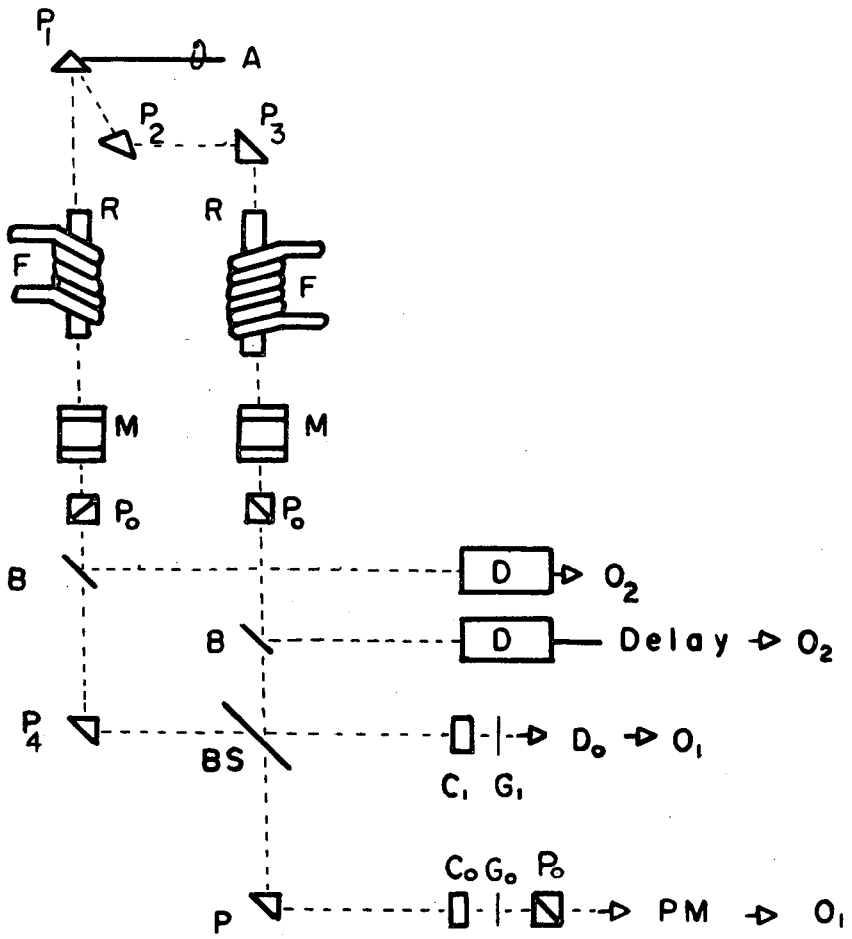

Fig. 10b Total Experimental Schematic. A = axis of rotation, B = microscope-slide beam splitter, BS = dielectric-coated beam splitter, C = nonlinear crystal, D = optical detector, D_o = far-infrared detector, F = flash lamp, G = filter, M^o = resonant reflector, P = prism, P_o = polarizer, PM = photomultiplier, O = oscilloscope, R = ruby rod. C_o is the sum-frequency crystal, C1 the difference frequency crystal. The oscilloscopes are Tektronix 519 (O_2) and 556 (O_1).

The far infrared signal is detected using a crystal of n-type InSb (Putley[35] detector) at T = 1.3°k in a magnetic field of 5500 Oe. It is biased with a constant voltage of 0.25 volts and the current is measured using an operational amplifier with a feedback resistor R_F = 205 kΩ. The response time of this system is 2 μsec. The sensitivity of the detector was measured using a black body at 200°C and a filter passing only 0-50 cm^{-1}. This showed the average noise equivalent power in a 5×10^5 Hz bandwidth to be 10^{-6} watts. However, since the sensitivity is certainly not uniform in this energy region[35] and since there are inevitable local system resonances at long wavelengths, the absolute values of the infrared power may be in error by an order of magnitude. For this reason, emphasis is on relative powers in our measurements.

Signals from the sum-frequency generation (1P28 photomultiplier output) and the difference-frequency generation are displayed simultaneously on a dual-beam oscilloscope (Tektronix 555 or 556). The scope is triggered by the laser pulses, via the 519 scope.

III. THEORETICAL APPARATUS

Summary of Contents

A list of the various aspects of a general calculation is presented. Values of nonlinear susceptibilities, effects of multi-mode lasers, and phase-matching are discussed. A calculation of power which includes the effect of finiteness of the beam is done in the following way: The laser beams produce a nonlinear polarization source of finite extent. The intensity of radiation produced by the nonlinear polarization is integrated over the collection system. This calculation is useful for simple cases. For the case where absorption, birefringence, or boundary conditions have appreciable effects, a more complete calculation is needed. For this case, we Fourier analyze the nonlinear polarization source and use an analysis of plane wave sources to obtain the total power collected.

III. THEORETICAL APPARATUS

The simple introductory calculation presented earlier has many obvious deficiencies. Any serious quantitative calculation has to include treatment of many factors not mentioned in the simple calculation. A comprehensive treatment of all aspects of the problem is out of the question. A fairly comprehensive listing of these aspects is as follows: (1) Numerical values of the nonlinear susceptibilities, their relation to electro-optic coefficients, and their dispersion relations, (2) possible depletion of the lasers, (3) effect of finite transverse cross-section and the resultant diffraction (this includes the effect of focussing the beam), (4) finite collection angle of detection system, (5) effect of the mode structure of the lasers, (6) local field effects, (7) boundary conditions at surfaces of crystals, (8) near-field effects, i.e., the effect of the size of the generating volume being only a few far ir λ's in extent, (9) incorporation of absorption, (10) effect of birefringence, (11) phase matching, both collinear and non-collinear, (12) lack of homogeneity of the crystals, and (13) effect of mode-locked pulses. This by no means represents a table of contents for this section. Some topics will be treated at some length; others will be ignored. Even the ordering is meaningless because of the interrelationships among them. Before launching into more general calculations, let us briefly discuss a few aspects which can be singled out conveniently.

Since there have been few experiments in difference frequency generation, we would be hard pressed to find values of the nonlinear susceptibility if it had no close relationship to other more familiar effects. Considerable work has been done in relating the susceptibilities

of various effects. Using assumed time-averaged free energies which were not rigorously correct, a set of permutation symmetry relations were derived.[36] A rigorous derivation[37] using quantum mechanical microscopic expressions for the nonlinear susceptibilities yields $\chi_{ijk}\ (\omega_3 = \omega_1 + \omega_2) = \chi_{jik}\ (\omega_1 = \omega_3 - \omega_2) = \chi_{kij}\ (\omega_2 = \omega_3 - \omega_1)$. This says that a difference frequency susceptibility is equal to a sum frequency susceptibility, with a juggling of indices and frequencies, but using the same set of frequencies. There is in general dispersion with respect to all three frequencies. If ω_2 is small, i.e., if there are no resonances near or below ω_2 and thus little dispersion below ω_2, then $\chi_{kij}\ (\omega_2 = \omega_3 - \omega_1) = \chi_{ijk}\ (\omega_3 = \omega_1 + \omega_2) \approx \chi_{ijk}(\omega_1 = \omega_1 + 0)$. Thus for most purposes, we could use $\chi\ (\omega = \omega + 0)$ to find our susceptibility. It will be recognized that this gives a polarization at the frequency of an incident field in addition to the linear polarization and thus gives a contribution to the index of refraction which is linearly dependent on an applied static electric field. This is the well-known and well-studied electro-optic effect. A little algebra[38] reveals the relationship

$$\chi_{j\ell k}\ (\omega'_{vis} = \omega_{vis} + \Omega) = \frac{\varepsilon_j \varepsilon_\ell}{4\pi}\, r_{j\ell k} \qquad (5e)$$

where $r_{j\ell k}\, E_k = \left(\Delta \frac{1}{n^2}\right)_{j\ell}$ and Ω is a low frequency.

Thus the electro-optic coefficients[39] carry over almost directly for difference-frequency experiments at low frequencies. At higher frequencies and for materials not studied electro-optically, one must go to calculations[49] involving some simple model. General quantum-mechanical expressions for susceptibilities are generally limited by the lack of knowledge of matrix elements. Calculations of susceptibilities

are important and interesting, but we will not treat them here.

Calculations are most easily done for given single-mode operation of each of the two lasers, i. e., for perfect spatial and temporal coherence. Ruby lasers are generally not perfectly coherent. The most obvious sign of multi-mode operation is the angular spread of the beam, which is considerably larger than the diffraction angle of a perfectly coherent beam. A coherent beam of cross-sectional area A and wavelength λ will have a divergence solid angle Ω such that $A\Omega/\lambda^2 \approx 1$. A typical ruby laser will have $A\Omega/\lambda^2 = N$ where N, the number of modes is on the order of 100. We shall first carry out calculations assuming single-mode laser beams.

Phase-matching requires that $\vec{k}_1 - \vec{k}_2 = \vec{k}$, for large difference-frequency output power. The length of the wave-vector $\vec{k}_i$ is equal to $\frac{\omega_i}{c} n_i$. Since the index of refraction is generally much larger at the low frequencies, $|\vec{k}|$ is generally larger than $|\vec{k}_1| - |\vec{k}_2|$. There are two ways to achieve the phase-matching: noncollinearly and collinearly. Since $|\vec{k}_1|$, $|\vec{k}_2|$ are much longer than $|\vec{k}|$, a small angle between $\vec{k}_1$ and $\vec{k}_2$ can easily make $\vec{k}_1 - \vec{k}_2$ sufficiently large (see Fig. 11). This is called non-collinear phase-matching. It does not require birefringence and can be used for large difference frequencies. Collinear phase-matching requires manipulation of the indices of refraction. Birefringence is a convenient means. Propagation along the optic axis yields $n_e = n_o$; n_e is the extraordinary and n_o the ordinary index of refraction. n_e moves away from n_o as the angle between the optic axis and the propagation direction increases, $|n_e - n_o|$ reaching a maximum at 90°. Using the larger index for the larger frequency ω_1, we can increase the

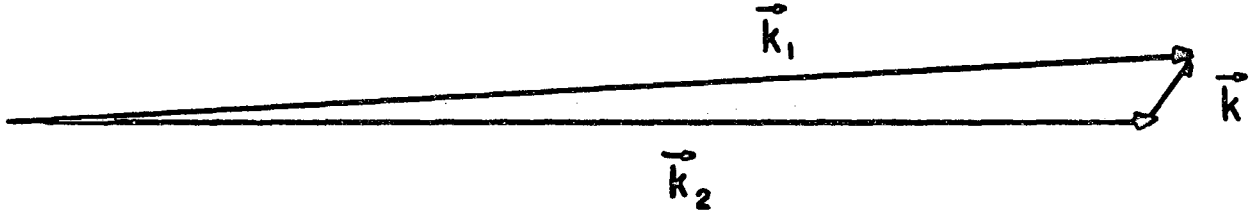

XBL 698-1124

Fig. 11 Noncollinear Phase-Matching (not to scale). The laser wave-vectors, $\vec{k}_1$ and $\vec{k}_2$, are several orders of magnitude longer than the far-infrared wave-vector $\vec{k}$.

collinear $|\vec{k}_1 - \vec{k}_2|$ from $\frac{n_o(\omega_1 - \omega_2)}{c}$ continuously to approximately $|n_e - n_o|\left(\frac{\omega_1}{c}\right)$. This is sufficient to phase-match low frequencies, but is generally limited to wave-numbers below 200 cm^{-1}. For example, using $LiNbO_3$ with $n_o - n_e \approx 0.08$ and n (infrared) ≈ 6.5 and ruby lasers as sources, we are limited to about 180 cm^{-1}.

A simple calculation which is much more useful than our introductory plane-wave calculation is as follows. Let us assume two beams as before, propagating in the z-direction and producing the nonlinear polarization (Eq. 1,2). However, let us confine the beams to a cylinder of radius a (The axis of the cylinder is the direction of propagation.) A nonlinear polarization of frequency $\omega = \omega_1 - \omega_2$ and wavevector $k_1 - k_2 = k + \Delta k = \frac{\omega}{c} n + \Delta k$ will be produced in the cylinder of radius a and length ℓ, the length of the nonlinear crystal. We neglect the effect of the boundary by assuming the detector is buried in a dielectric medium which matches the index of refraction of the nonlinear medium (see Fig. 12). We want to integrate over the contributions of the polarization wave in the far field approximation to find the radiation field at the detector. The general expression for this is

$$\vec{E}(\vec{r},t) = \frac{\omega^2}{c^2} \int \left(\vec{\vec{I}} - \hat{s}\hat{s}\right) \cdot \vec{P}(\vec{r}'t) \frac{\exp(ik|\vec{r} - \vec{r}'|)}{|\vec{r} - \vec{r}'|} d^3r' \qquad (5f)$$

where $\vec{r}'$ varies over the source region, $\vec{r}$ over the detection region, $\vec{\vec{I}}$ is the unit tensor and $\hat{s}$ is the unit vector in the direction of $\vec{r} - \vec{r}'$. To compute the integral we assume that the angular dependence of $(\vec{\vec{I}} - \hat{s}\hat{s})\cdot\vec{P} = P\,(\text{transverse})$ is small, that $|\vec{r} - \vec{r}'| = r$ in the demominator, and that $|\vec{r} - \vec{r}'| = r - \frac{\vec{r}'\cdot\vec{r}}{r}$ in the exponent. The assumption on the angular dependence is justifiable if $\vec{P}$ is roughly perpendicular to $\hat{s}$

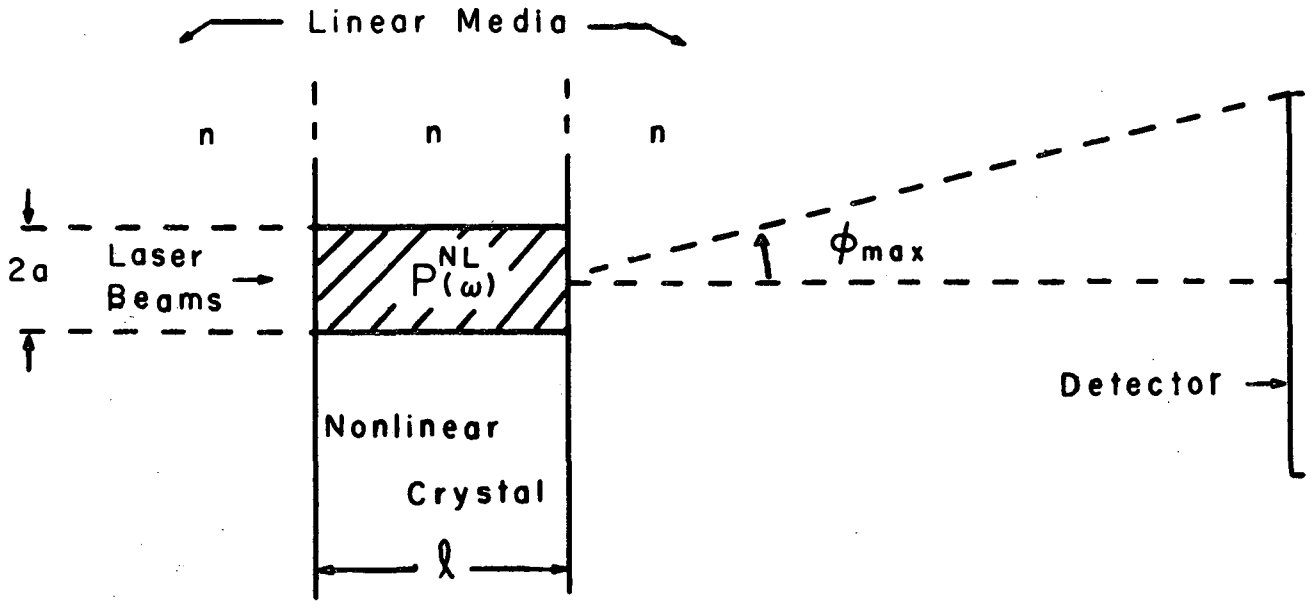

XBL 698-1125

Fig. 12 Schematic for Calculations of Power Output. The laser beams produce a nonlinear polarization in the crystal at the difference frequency; the polarization is then treated as a source for the difference-frequency generation.

and the integration is over angles small with respect to $\pi/2$ inside the crystal (the cosine function varies slowly near zero). Integrating the Poynting vector over the detector yields the total far infrared power W collected by the detection system.

$$W = \frac{n\omega^4}{4c^3} |\chi_D^{(2)}|^2 |\mathcal{E}_1|^2 |\mathcal{E}_2|^2 \ell^2 (\pi a^2)^2 \int^{\Phi \max} \sin\Phi \, d\Phi \left[\frac{\sin \eta}{\eta}\right]^2 \left[\frac{2J_1(\beta)}{\beta}\right]^2 \qquad (6)$$

where $\eta = \frac{k\ell}{2}(1 + \frac{\Delta k}{k} - \cos \Phi)$, $\beta = ka \sin \Phi$, Φ is the angle between the incoming beams and the generated radiation, and Φ max is the maximum angle collected in the detection system.

The two terms in the integral represent the phase-matching term and the diffraction from a circular aperture. If the beam radius a is large so that the angular spread is small, the Bessel function diffraction term will be large only for small Φ, $\Phi \lesssim \frac{1}{ka}$; the phase-matching term will be approximately constant for small Φ and may be taken outside the integral. When we are collecting essentially all of the output (Φ max >> $\frac{1}{ka}$), then the integral becomes on the order of $\frac{1}{k^2a^2}$. We thus obtain the same functional form we obtained in the plane-wave approximation.

We have assumed here a distant detector covering some finite area. What is our actual detection system? We have a light pipe entrance near the nonlinear crystal. The power entering the pipe is proportional to $\int_R |E(r)|^2 d^2r$, where R is the spatial extent of the opening into the pipe. If the beam is smaller than the opening and the pipe is placed close to the crystal, essentially all of the radiation enters the pipe and Parseval's theorem applies. Thus the power entering the pipe is proportional to $\int |\mathcal{E}(k)|^2 d^2k$, where the integral is over all directions of $\vec{k}$. ($\mathcal{E}(k)$ is the Fourier transform of E(r).) However,

the pipe is tapered, essentially focusing the radiation onto the detector, so that radiation entering at too large an angle will not reach the detector. Thus, there is an angular cutoff, a maximum transverse wave vector, $k_{\perp\,max}$, beyond which radiation is not detected. The power detected is proportional to $\int^{k_{\perp}max}|\&(k)|^2\, d^2k$. One can show that this integral leads to the same expression as Eq. 6. Physically, this is true because the field $E(\vec{r})$ at a point $\vec{r}$ far away from the small source is given approximately by $\&(\vec{k})\exp(i\vec{k}\cdot\vec{r})$ with $\vec{k}$ parallel to $\vec{r}$. Calculations with Fourier components in the k-space often turns out to be simpler and more straightforward. Such a calculation follows.

The general approach is as follows. The Fourier components of the nonlinear polarization in the crystal are found from the Fourier components of the incoming field. The plane-wave solutions for each Fourier component are calculated in a slab, including absorption and boundary conditions. (The slab is assumed infinite in the transverse dimensions since the nonlinear polarization is confined to the beam size and is not affected by the boundaries in the transverse direction except by reflections.) The electric field amplitude is constructed from its Fourier components, and its absolute square is integrated over the spatial aperture R to obtain the power. In general, there is a cutoff in k-space also because the detector system can only accept radiation in a definite solid angle, so that the power is proportional to

$$\int_R \left|\int^{k_{\perp}max} \&(k)e^{\,i\vec{k}\cdot\vec{r}}\, d^2k\right|^2 d^2r.$$

In the case where essentially all of the radiation enters the aperture, this is simplified (as discussed above) to the much simpler integral

$\int^{k_{\perp}\,max} \left|\mathcal{E}(k)\right|^2 d^2k.$

Let us proceed by finding the plane-wave solutions with absorption and boundary conditions. Let us assume a slab of nonlinear medium with boundaries perpendicular to the z-axis. (This is a definition of the z-direction and has nothing to do with the c-axis of a crystal, which may be arbitrarily oriented.) Let us consider an ordinary ray; thus ε can be treated as a scalar. The wave equation and Maxwell's equations take the form

$$\nabla \times \nabla \times E - \frac{\varepsilon\omega^2}{c^2} E = \frac{4\pi\omega^2}{c^2} P^{NLS}$$

$$\nabla \cdot D = \nabla \cdot (\varepsilon E + 4\pi P^{NLS}) = 0 \qquad (6a)$$

for a non-magnetic, charge-free, current-free medium. P^{NLS} takes the form of $P \exp(i \vec{k}_s \cdot \vec{r})$ where $\vec{k}_s$ is given by $\vec{k}_1 - \vec{k}_2$ (see Eq. 2) and may in general be complex if there is absorption of the laser radiation by the medium. Letting $E = \mathcal{E}(\vec{k},z)e^{i\vec{k}\cdot\vec{r}}$, $k^2 = \frac{\varepsilon\omega^2}{c^2}$ and assuming $|\vec{k}_s - \vec{k}| \ll k$, the wave equation transforms to

$$-2ik_z \frac{\partial \mathcal{E}}{\partial z} = \frac{4\pi\omega^2}{c^2} P_{\perp} e^{i\Delta kz} \exp(\frac{\alpha}{2} - \alpha_L)z \qquad (7)$$

where $\Delta k = \mathrm{Re}\,(k_z - k_{sz})$, $\frac{\alpha}{2} = \mathrm{Im}\, k$, $\frac{\alpha_L}{2} = \mathrm{Im}\, k_1 = \mathrm{Im}\, k_2$, and $P_{\perp}$ is the component of P perpendicular to $\vec{k}_s$. The condition •, $|\vec{k}_s - \vec{k}| \ll k$, is a condition which is experimentally desirable in order to obtain higher power input; that is, phase-matching over a distance of many wavelengths and absorption lengths being much greater than a wavelength. $P_{\perp}$ may have a z-dependence, in which case we must return to equation (7) for any given functional dependence. The case of $P_{\perp}$ being constant occurs

frequently enough to warrant writing the result:

$$|\mathcal{E}|^2 = \left[\frac{2\pi\omega^2}{c^2|k_z|}\right]^2 |P_1|^2 \frac{1 + e^{(\alpha - 2\alpha_L)z} - 2\cos \Delta kz e^{\left(\frac{\alpha}{2} - \alpha_L\right)z}}{(\Delta k)^2 + \left(\frac{\alpha}{2} - \alpha_L\right)^2} \tag{8}$$

This result is a solution to the inhomogeneous wave equation which goes to zero at z = 0. This agrees with the result of Bey, Giuliani, and Rabin[41] for a similar case.

Now let us include the boundary conditions. The situation is pictured in Fig. 13. We assume the following forms for the electric fields:

$$\begin{aligned} E_1 &= [\mathcal{E}_1 + f(z)]\, e^{in'\vec{k}_1\cdot\vec{r}}\, e^{-\frac{\alpha}{2}z} \\ E_2 &= \mathcal{E}_2\, e^{in'\vec{k}_2\cdot\vec{r}}\, e^{-\frac{\alpha}{2}(\ell - z)} \\ E_3 &= \mathcal{E}_3\, e^{i\vec{k}_3\cdot\vec{r}},\quad E_4 = \mathcal{E}_4\, e^{i\vec{k}_4\cdot\vec{r}} \end{aligned} \tag{8a}$$

where E_1 and E_2 are respectively the forward and backward propagating electric field inside the crystal, E_3 and E_4 are respectively the reflected and transmitted electric fields outside the crystal, $\tilde{n} = n' + in''$ is the index of refraction of the material, $|k_i| = \omega/C$, and $f(z)$ is a solution to the inhomogeneous wave equation chosen such that $f(0) = 0$. In the same approximation as before, Δk, $\alpha \ll k$, we can find H or B from Maxwell's equations, match the boundary conditions[54] for E and H, thereby finding $\mathcal{E}_4$ as a simple function of $f(\ell)$. The case with $\mathcal{E}$ perpendicular to the plane of incidence is distinct from the

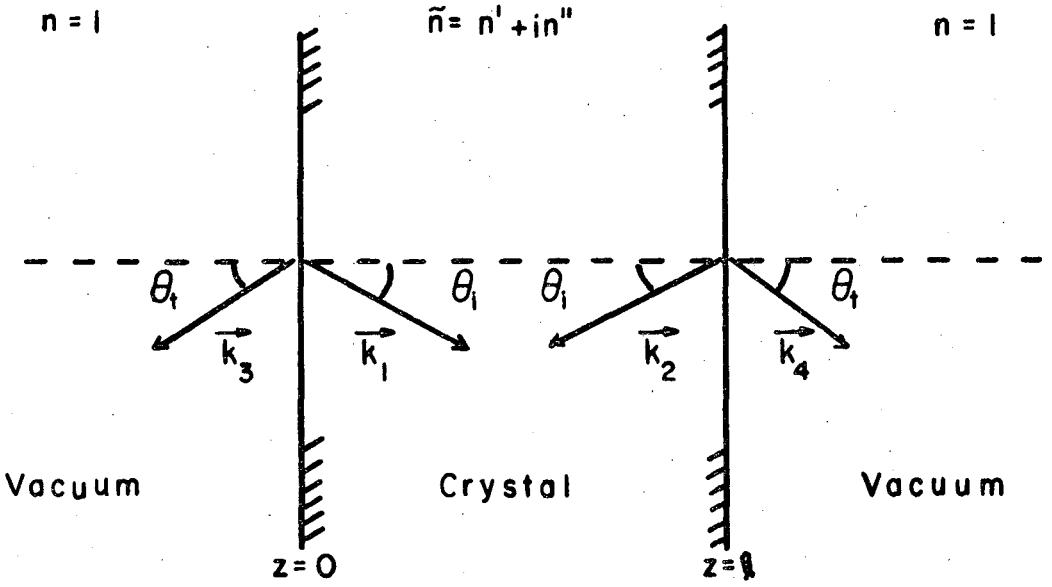

XBL 698-1126

Fig. 13 Four Waves in a Crystalline Slab. Four waves generated at the difference frequency inside and outside the slab of a nonlinear crystal.

parallel case. The results are

$$\mathcal{E}_{4\perp} = f(\ell)\, e^{-(\alpha/2)\ell}\, e^{\left[i\Phi\ \frac{1 + r_\perp}{1 - r_\perp^2\, e^{-\alpha\ell}\, e^{2ik_z\ell}}\right]}$$

$$\mathcal{E}_{4\parallel} = \tilde{n}\, f(\ell)\, e^{-(\alpha/2)\ell}\, e^{\,i\Phi\left[\frac{1 + r_\parallel}{1 - r_\parallel^2\, e^{-\alpha\ell}\, e^{2ik_z\ell}}\right]} \tag{9}$$

where

$$r_\perp = \frac{\tilde{n}\cos\theta_i - \cos\theta_t}{\tilde{n}\cos\theta_i + \cos\theta_t}$$

$$r_\parallel = \frac{\cos\theta_i - \tilde{n}\cos\theta_t}{\cos\theta_i + \tilde{n}\cos\theta_t}$$

$$k_z = k_{1z} n'$$

and Φ is just a phase factor. The absolute squares of these quantities are of interest.

$$|\mathcal{E}_{4\perp}|^2 = \frac{|f(\ell)|^2\, e^{-\alpha\ell}\, (1 + r_\perp)^2}{(1 - r_\perp^2\, e^{-\alpha\ell})^2}\left[1 + \frac{4r_\perp^2\, e^{-\alpha\ell}}{(1 - r_\perp^2\, e^{-\alpha\ell})^2}\sin^2 k_z\ell\right]^{-1}$$

$$|\mathcal{E}_{4\parallel}|^2 = \frac{|f(\ell)|^2|\tilde{n}|^2\, e^{-\alpha\ell}\, (1 + r_\parallel)^2}{(1 - r_\parallel^2\, e^{-\alpha\ell})^2}\left[1 + \frac{4r_\parallel^2\, e^{-\alpha\ell}}{(1 - r_\parallel^2\, e^{-\alpha\ell})^2}\sin^2 k_z\ell\right]^{-1} \tag{10}$$

The terms in the brackets are precisely the form for transmission in Fabry-Perot interferometers. Thus we can see a resonance effect due to the spacing of the two boundaries of the crystal.

Now we want to find what the plane-wave nonlinear polarization sources are for given laser inputs. For as much generality as we can handle, let us assume focused beams with Gaussian transverse cross-section. An unfocused beam is a special case of the focused beam. We first find the general form of such beams within the crystal. Combining the two electric fields to form the nonlinear polarization, we get a polarization source as a spatial function. The transverse Fourier transform yields the plane-wave sources which our formalism above requires. This is similar to a calculation for second-harmonic generation by Bjorkholm.[42]

First we want to describe the laser beam within the crystal. In general, one might have the crystal interface at any point along the beam, at any distance from the focal point. One might then describe the laser in vacuo or air and treat refraction at the crystal boundaries. Since refraction is not linear but follows Snell's law, the minimum beam radius and thus the beam spread inside the crystal would depend on the position of the interface. However, in the regime where the focal spot size is many laser wave lengths, the difference is insignificant.[43] (The diffraction angle Φ is small, $\sin \Phi \approx \Phi$, and refraction is nearly linear.) This is necessarily satisfied for most far-infrared experiments because we want the beam radius to be larger than the far-infrared wave length to keep the far-infrared diffraction angle small enough for collection in a detection system. The fact that the difference-frequency wave length is much longer than optical wave lengths, scaling up diffraction accordingly, forces us to have small angular spread of the laser, $k_T/k \ll 1$ where k_T is

transverse wavevector. Thus we will treat the laser as if it were in air, introducing the crystal later without changing the focal spot size.

In the focal plane, at z = 0, the electrical field with a given polarization and a Gaussian intensity profile is given by

$$E\,(x,y,\,z=0,\,t) = E_\omega \exp\left[\left[-(x^2+y^2)/w_o^2\right] - i\omega t\right]. \qquad (10a)$$

The beam focal spot radius is w_o, defined as the radius at which the intensity falls to e^{-2} times its value on axis.

The field at other points in space can be found by Fourier analysis of the focal plane distribution $E(x,y,z=0,t)\exp[ik_z z]$, which yields a sum of plane waves of the form $\mathcal{E}(k_x^o, k_y^o, k_z^o)\exp[i\vec{k}^o\cdot\vec{r} - i\omega t]$ with $(k^o)^2 = (k_x^o)^2 + (k_y^o)^2 + (k_z^o)^2 = \omega^2/c^2$. Fourier analysis of the focal plane distribution of the electric field amplitude gives

$$\mathcal{E}(k_x^o,k_y^o,k_z^o) = E_\omega \sqrt{2\pi}\left(\frac{1}{2}w_o^2\right) \exp\left[-\frac{w_o^2 k_T^{o2}}{4}\right] \delta\left[k_z^o - \left(k^{o2} - k_T^{o2}\right)^{\frac{1}{2}}\right] \qquad (11)$$

where $k_T^2 = k_x^2 + k_y^2$ and $\delta(x)$ is the Dirac delta function. The delta function relating k_z^o, k_T^o, and k^o represents an approximation inasmuch as there are values of k_T^o greater than k^o. This means that the focal plane distribution cannot be represented strictly by a group of monochromatic plane waves. However, as long as the Fourier components associated with $k_T > k^o$ are very small, our approximation is very good. The requirement is $\frac{1}{2}k^o w_o \gg 1$ or $k_T^o/k^o \ll 1$ for k_T^o with appreciable Fourier components. This is equivalent to the condition that the

transverse dimension of the beam is much larger than a wave length.

Inversion of Eq. (11) is easy, assuming $k_T^o/k^o \ll 1$.

$$E(x,y,z,t) = \frac{E_\omega e^{ik^o z}}{1 + i\xi} \exp\left[-\frac{(x^2 + y^2)(1 - i\xi)}{w_o^2 (1 + \xi^2)}\right] \qquad (12)$$

where $$\xi = \frac{2z}{kw_o^2} \equiv z/Z_R.$$

This is the expression for the electric field of the beam in all space, assuming no interfaces. All details are specified by the single parameter w_o. This form has been obtained using confocal resonator theory.[44,45] An unfocused beam is specified by the same form. The divergence of the beam specifies w_o and the beam radius at the point of interest, with the divergence, specifies the distance to the fictitious focal plane.

The radius of the beam is

$$w(z) = w_o(1 + \xi^2)^{1/2}. \qquad (12a)$$

The length parameter $Z_R = \frac{1}{2} kw_o^2$, called the Rayleigh range in antenna theory, is the value of z for which the power density falls to half of its value at the focal plane.

Now let us consider placing a crystal interface at $z = z_o$. At the interface, the tangential components of $\vec{k}$ will be continuous. The normal component will change according to the index of refraction, which will depend on direction in the case of an extraordinary ray. Thus, for $z > z_o$, assuming E parallel to the surface, we can write

$$\mathcal{E}(k_x,k_y,k_z) = E_\omega \sqrt{2\pi}\left(\frac{1}{2}w_o^2\right) \exp\left[-\frac{w_o^2 k_T^2}{4}\right]$$
$$\times \delta\left[k_z - (k^2 - k_T^2)^{\frac{1}{2}}\right] \exp\left(-ik_z z_o + ik_z^o z_o\right) \qquad (13)$$

where $k = \frac{\omega}{c} n$ and n, the index of refraction, can depend on direction for extraordinary rays.

Now we wish to invert Eq. (13) for both extraordinary and ordinary wave propagation, again dropping high order powers of k_T/k. For ordinary rays, k is simply given by $\frac{\omega}{c} n_o$. For the extraordinary ray, we need the directional dependence. Defining the x-direction such that the optic axis is in the x - z plane we may write

$$k = k' + \frac{2\cos\theta \sin\theta\,(n_o - n_e)}{n'} k_x \equiv k' + \zeta k_x \qquad (14)$$

where $k' = \frac{\omega}{c} n_e(\theta) \equiv \frac{\omega}{c} n'$ is the wave-vector at normal incidence to the interface, at angle θ to the optic axis; n_o and n_e are respectively the ordinary and extraordinary indices of refraction.

The result of inversion for the ordinary rays inside the crystal (within a constant phase factor) is

$$E(r) = \frac{E_\omega e^{ikz}}{1 + i\xi} \exp\left[-\frac{(x^2 + y^2)(1 - i\xi)}{w_o^2 (1 + \xi^2)}\right] \qquad (15)$$

where $\xi = \frac{2(z - z_o)}{k w_o^2} + \frac{2z_o}{k^o w_o^2}$. For the extraordinary polarization, we have

$$E(r) = \frac{E_\omega e^{ik'z}}{1 + i\xi'} \exp\left[\frac{\left\{[x + \zeta(z - z_o)]^2 + y^2\right\}(1 - i\xi')}{w_o^2 (1 + \xi'^2)}\right] \qquad (16)$$

where $\xi' = \frac{2(z - z_o)}{k' w_o^2} + \frac{2z_o}{k^o w_o^2}$. We want to combine one ordinary and one extraordinary wave to make a polarization wave which is phase-matchable. We will assume two frequencies $\omega_1 > \omega_2$, producing a polarization wave at $\omega = \omega_1 - \omega_2$. Which frequency component is to be ordinary depends on whether the crystal is negative, positive, or uniaxial, but the calculation is really the same. We assume ω_1 to be the ordinary wave, ω_2 the extraordinary and want a polarization of the form of Eq. (2). The form is reduced by neglecting terms which are small for reasonable experiments. For example, $|\xi(\omega_1) - \xi'(\omega_2)| \ll 1 + \xi(\omega_1)\,\xi(\omega_2)$ is valid for visible or near-visible light sources, difference frequencies less than or on the order of 100 cm^{-1}, and beam spreads with $k_T/k \ll 1$. Similarly, $\frac{\xi_1 (k_1 - k_2')}{k_1} \ll 1$ requires that we are not too far out of the Rayleigh range, i. e., we do not let the beam diffract too much. These are all reasonable limitations.

The result is

$$P(\vec{r}) = \frac{2\, d\, E_{\omega_1} E^*_{\omega_2}}{1 + \xi^2} e^{i(k_1 - k_2')z} \exp\left[\frac{-\zeta^2 z'^2}{2w_o^2(1 + \xi^2)}\right] \exp\left[\frac{-2i\zeta z'\xi(x + \frac{\zeta z'}{2})}{w_o^2(1 + \xi^2)}\right]$$

$$\times \exp\left[\frac{-2(x + \frac{\zeta z'}{2})^2}{w_o^2(1 + \xi^2)}\right] \exp\left[\frac{-2y^2}{w_o^2(1 + \xi^2)}\right] \qquad (17)$$

where $z' = z - z_o$. The transverse Fourier transform is

$$P(k_T, z') = \frac{\chi\, E_{\omega_1} E^*_{\omega_2}}{2} w_o^2\, e^{i(k_1 - k_2')z}\, e^{ik_x \zeta z'/2}$$

$$\times \exp\left[-\frac{\zeta^2 z'^2}{2w_o^2} - \frac{k_T^2 w_o^2 (1 + \xi^2)}{8} - \frac{k_x \zeta z' \xi}{2}\right] \qquad (18)$$

The calculation of $f(\ell)$ [Eq. 9] is then carried out by finding the particular soltuion of the differential equation [Eq. 7] for each Fourier component of P_1. The field components parallel and perpendicular to the plane of incidence are calculated separately, subject to the appropriate boundary conditions [Eq. 10]. Finally, to find the total power detected, assuming that all the far infrared radiation goes into the collecting light pipe, we simply integrate the output from the crystal, $|\mathcal{E}(k)|^2$, over the solid angle collected in the detection system. The calculation is clear in principle but too lengthy to write out in detail. It must be carried out numerically by computer, except under extreme simplifying assumptions. Results of some numerical calculations are discussed in the next section.

IV. RESULTS OF EXPERIMENTS AND COMPARISON WITH THEORY

A. Summary of Experimental Results

For quick reference, a summary of experimental results are presented here without discussion. Fig. 14 shows oscilloscope traces of the laser pulses with corresponding outputs of the difference-frequency and sum-frequency detectors. The peak powers obtained at phase-matching were: 1 milliwatt at 8.1 cm^{-1} in 0.047 cm $LiNbO_3$, 20 milliwatts at 8.1 cm^{-1} in 1.5 cm $LiNbO_3$, 5 milliwatts at 29 cm^{-1} in 0.15 cm $LiNbO_3$. The variation of the power of the difference frequency output of the 1.5 cm $LiNbO_3$ crystal at 8.1 cm^{-1} as a function of the angular deviation from the phase-matched angle is shown in Fig. 15. The corresponding curve for 29 cm^{-1} generation in the 0.15 cm $LiNbO_3$ crystal is shown in Fig. 16. The respective phase-matching angles are 9.5° and 18.2° from the c-axis.

Signals were detected down to a frequency of 1.2 cm^{-1}, giving us ranges of tunability from 1.2 cm^{-1} to 8.1 cm^{-1} and 21 cm^{-1} to 37 cm^{-1}. The frequency of the output was verified by measurement with a far-infrared Fabry-Perot interferometer. Transmission curves for the lower frequency range (6.4 and 8.1 cm^{-1}) are shown in Fig. 17, for the higher frequency range (28.8 and 35.8 cm^{-1}) in Fig. 18. These curves indicate a half-angular divergence at the Fabry-Perot of greater than or equal to 30° for the 8.1 cm^{-1} case; it is considerably less than 30° for the higher frequency range.

Comparison of power outputs in $LiNbO_3$ and quartz gives an estimate of the relative electro-optic coefficients: $r_{22}(LiNbO_3)$: $r_{62}(\text{quartz}) \approx 8.5$.

Fig. 14. Correlation between Time Overlap of Laser Pulses and Strength of Sum and Difference Frequency Signals. The laser signals are displayed on a single oscilloscope trace (a) with one laser being delayed by 125 nsec. Sum frequency signals (b) and difference frequency signals (c) are displayed on a dual beam oscilloscope. Larger time overlap (upper) results in larger sum and difference frequency signals. The difference frequency signals correspond to a peak power of about one milliwatt.

Fig. 15. Phase-Matching Curve for 8.1 cm^{-1} in 1.5 cm $LiNbO_3$ Crystal. Variation of the power of the difference frequency signal as a function of the angular deviation from the phase-matched angle. The angles refer to the inside of the crystal.

Fig. 16. Phase-Matching Curve for 29 cm^{-1} in 0.15 cm $LiNbO_3$ Crystal. The dashed line is $\left(\frac{\sin\eta}{\eta}\right)^2$ the theoretical curve for no absorption. The solid line is the theoretical curve including absorption, $\alpha = 18\ cm^{-1}$.

Fig. 17. Fabry-Perot Scan of Difference-Frequency Output. The upper scan (a) is for a temperature difference $\Delta T = 60°C$ of the two lasers. For the lower scan (b), $\Delta T = 47°C$. The theoretical curves are Airy functions, calculated from the geometrical properties of the Fabry-Perot reflectors and averaged to account for the 30° collection half-angle.

Fig. 18. Fabry-Perot Scan of Difference-Frequency Output Using R_1 and R_2 Lines. The first scan (a) shows a difference frequency of 28.8 cm^{-1}; the second scan (b) shows 35.8 cm^{-1}.

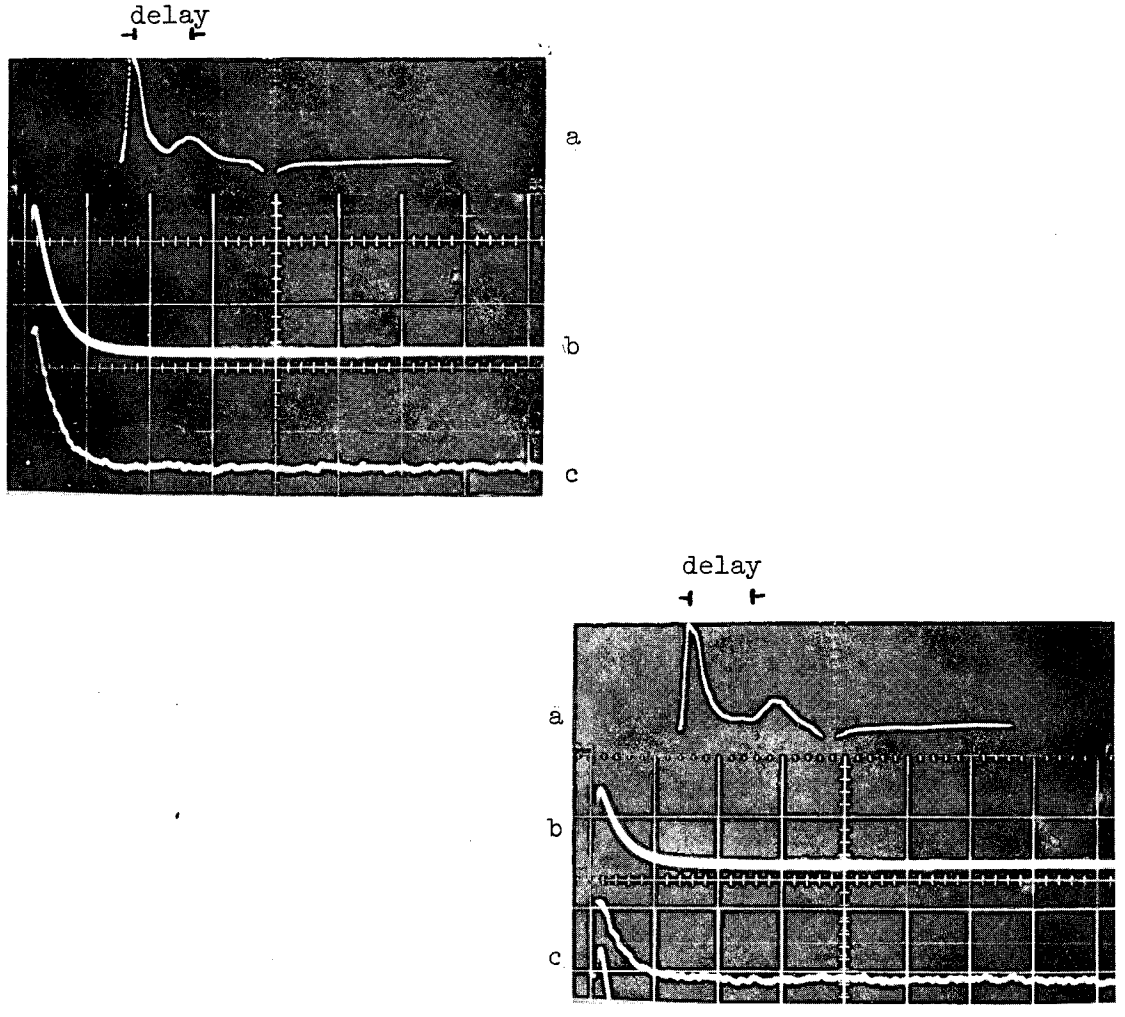

XBB 697-4898-A

Fig. 14

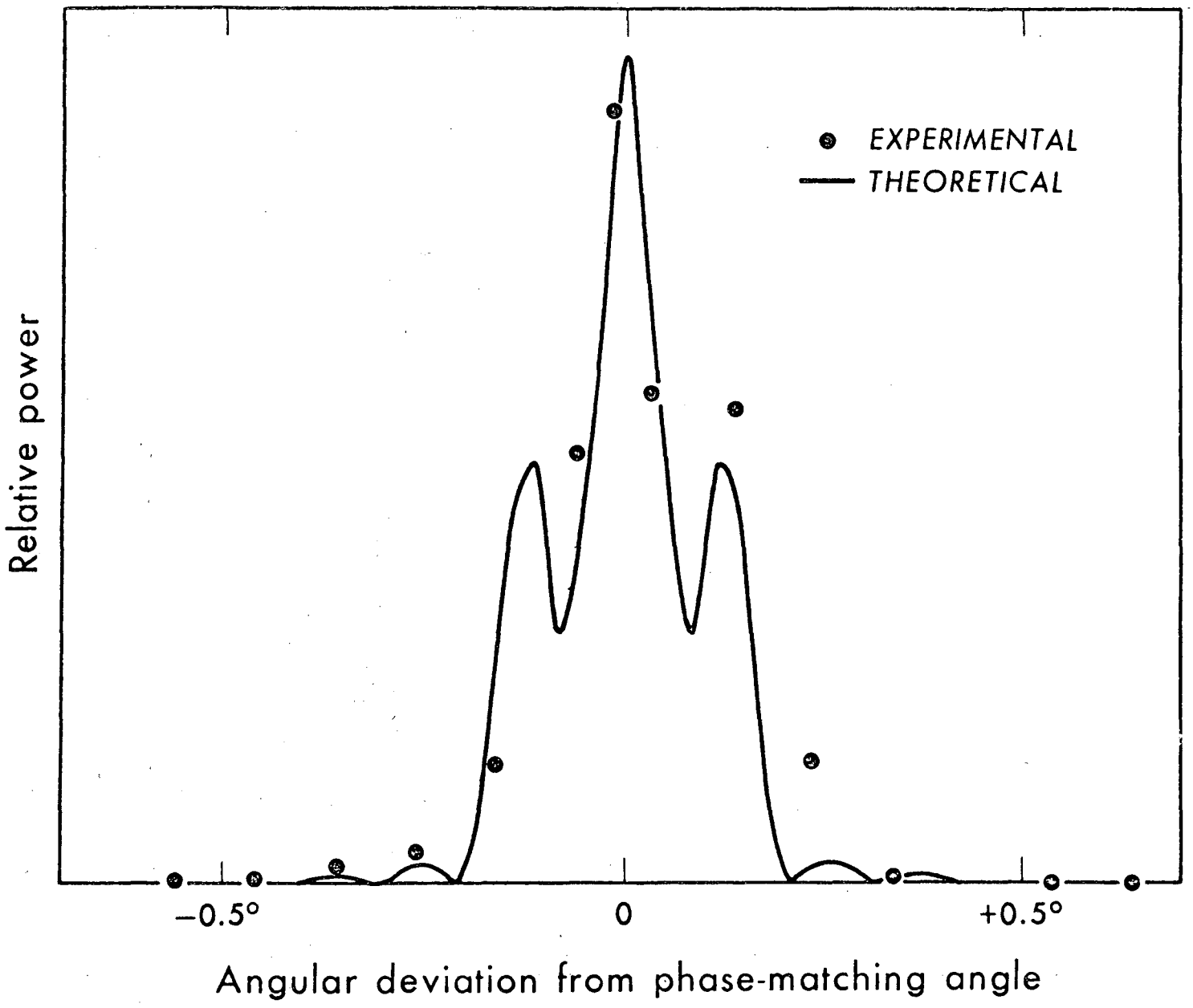

XBL 698-1128

Fig. 15

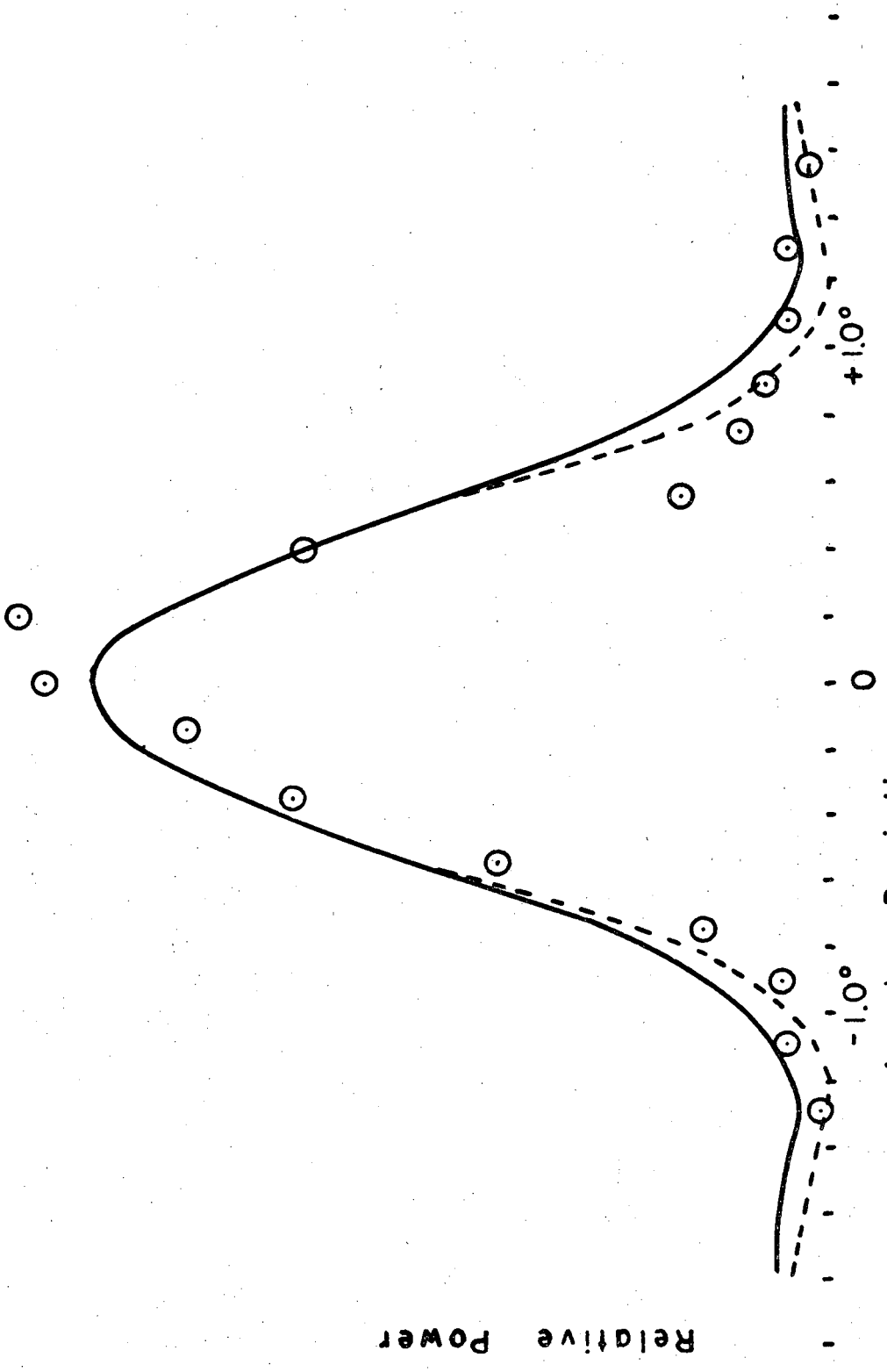

XBL 698-1127

Fig. 16

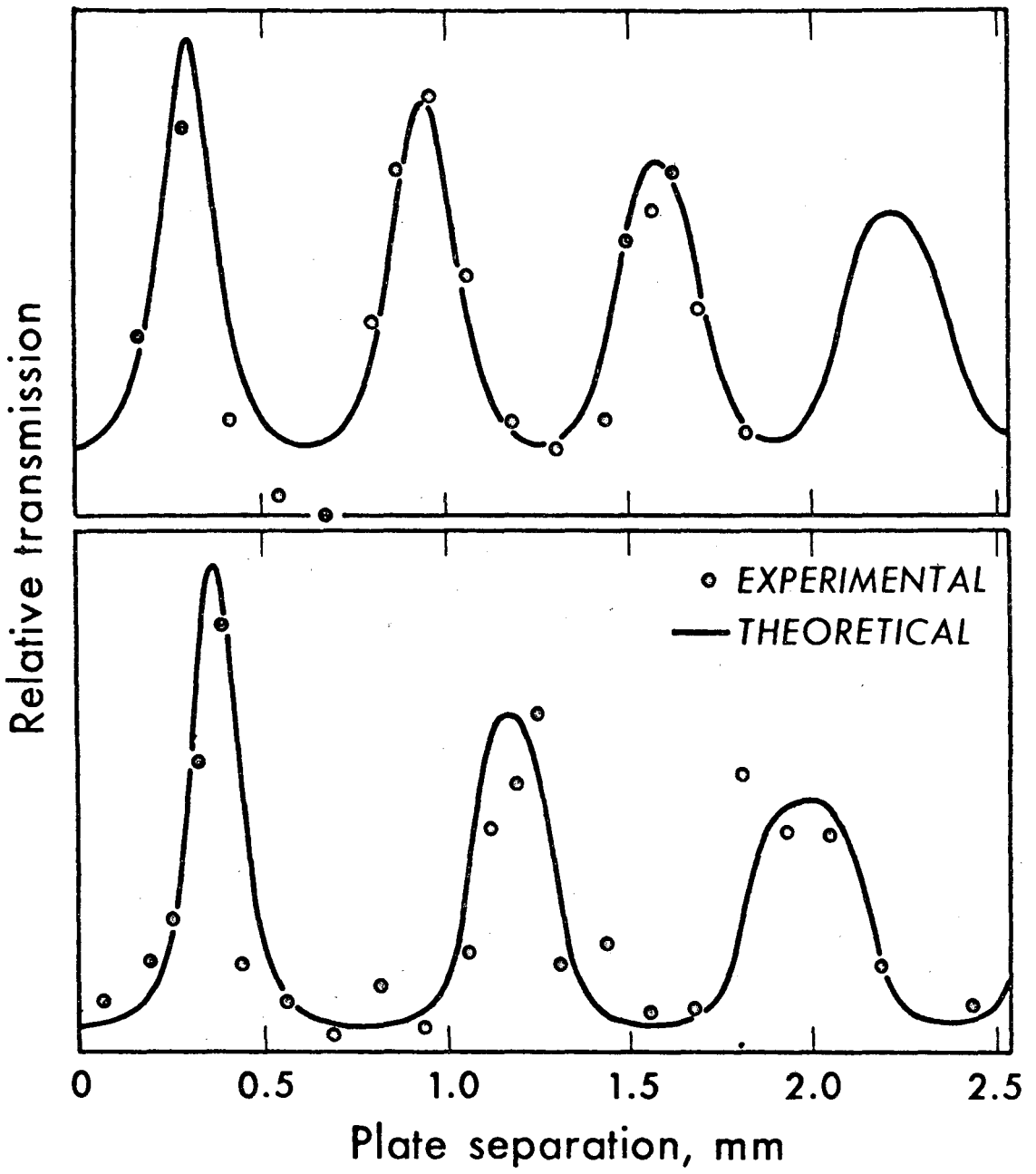

XBL 698-1129

Fig. 17

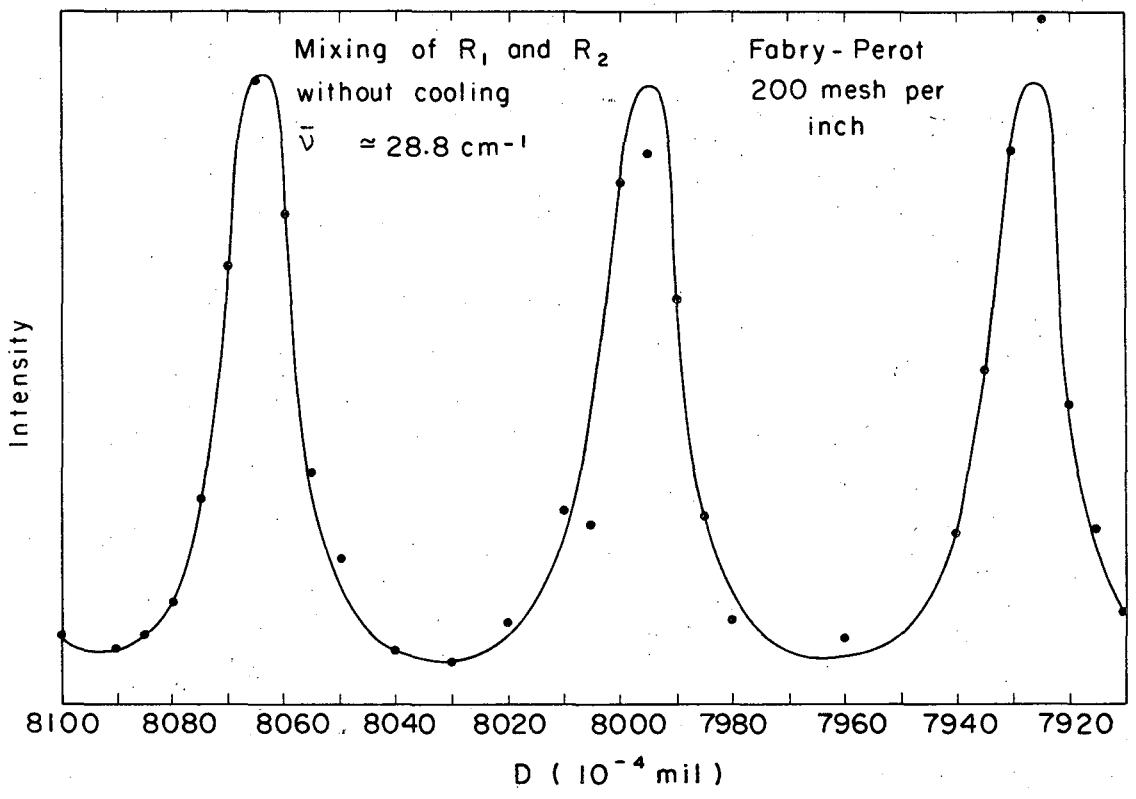

XBL693- 2226

Fig. 18a

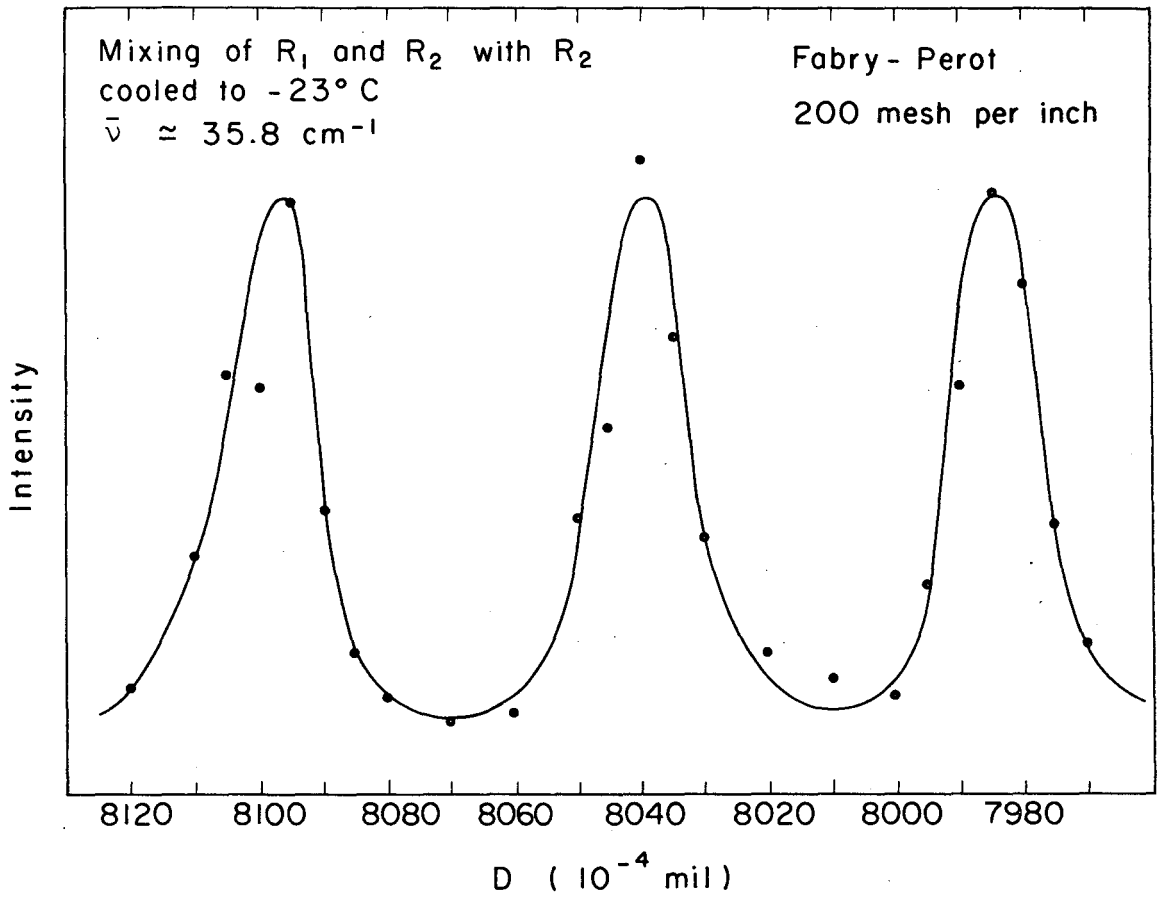
Mixing of R_1 and R_2 with R_2
cooled to -23° C
$\bar{\nu} \simeq 35.8\ cm^{-1}$
Fabry - Perot
200 mesh per inch
Intensity
8120
8100
8080
8060
8040
8020
8000
7980
D (10^{-4} mil)
XBL693 - 2224

Fig. 18b

B. Comparison with Theory

Let us first consider the experiment using two crystals of different thickness. Our crystals were of lithium niobate, $LiNbO_3$, thickness 0.047 cm and 1.5 cm. The lasers, operated on the R_1-transition, were separated in temperature by 60°C., corresponding to 8.1 cm^{-1} for the difference frequency.[16] The power obtained from the 0.047 cm crystal was about 1 milliwatt, in approximate agreement with a calculation using Eq. (6), including effect of mode structure, for typical laser pulses as input. The power was calculated for single-mode lasers with power and angular divergence corresponding to single modes within the multimode lasers. The result was then multiplied by the number of modes to give the total power. Power, rather than field amplitude, are added because of the incoherence. The 1.5 cm crystal yielded about 20 milliwatts, experimentally. The plane-wave theory suggests a z^2-dependence of power versus length, implying a ratio of about 1000:1 for the power output from the two crystals, compared to the experimental 20:1. A computer calculation using the formalism presented in the last section yielded a ratio of 60:1 when applied to the single difference-frequency 8.1 cm^{-1}. Let us consider the various effects involved here.

There are three effects, besides the fluctuations of the normalization process and possible local resonances at long wave lengths in the detection system, which should be kept in mind in any experiment comparing powers. The first is long-term changes in the sum-frequency output. The crystal used (KDP) is water soluble; thus surfaces are damaged by exposure to air. A comparison of power overlaps of the two

lasers and thus of the expected difference-frequency power output can not be done reliably by this method over long periods of time. Perhaps more important is the alignment of the two lasers. A small misalignment, say 10 minutes of arc, has no effect on the non-phase-matched sum-frequency generation, but may cut the difference-frequency generation almost completely. This again makes any long-term comparison difficult. With care in alignment and some luck with the reproducibility of the lasers, these problems represent at worst a factor of two uncertainty. The third effect, inhomogeneities of the crystal, may be worse. They may be present due to the crystal-growing process[46] or may be induced by the lasers.[47] Yajima and Inoue[12] have tried to include this effect in the effect of beam divergence, measuring the beam divergence after traversal of the crystal. Byer[48] has used the second-harmonic power and phase-matching curve to help choose crystals with minimum inhomogeneity. We have not included this effect in our calculations.

The various effects involved in the calculations are intermingled in the equations, but it is worthwhile to try to sort them out for discussion. First let us consider the effect of the boundary conditions. The index of refraction at 8.1 cm^{-1} is 6.55[49] at phase-matching. This yields a reflectivity r^2 at normal incidence of 0.54. The factor in the denominator of the Fabry-Perot factor [Eq. 10] becomes, with small absorption, $\frac{4r^2}{(1 - r^2)^2} = 10.2$. Thus we see that the output with plane-waves and a slab goes up as the square of the length but with deep modulations, the peaks being about 10 times the valleys [Fig. 19]. In a long crystal, two effects will average this out. First, the absorption coefficient[50] of $LiNbO_3$ at 8.1 cm^{-1} is about 1.4 cm^{-1}. The factor

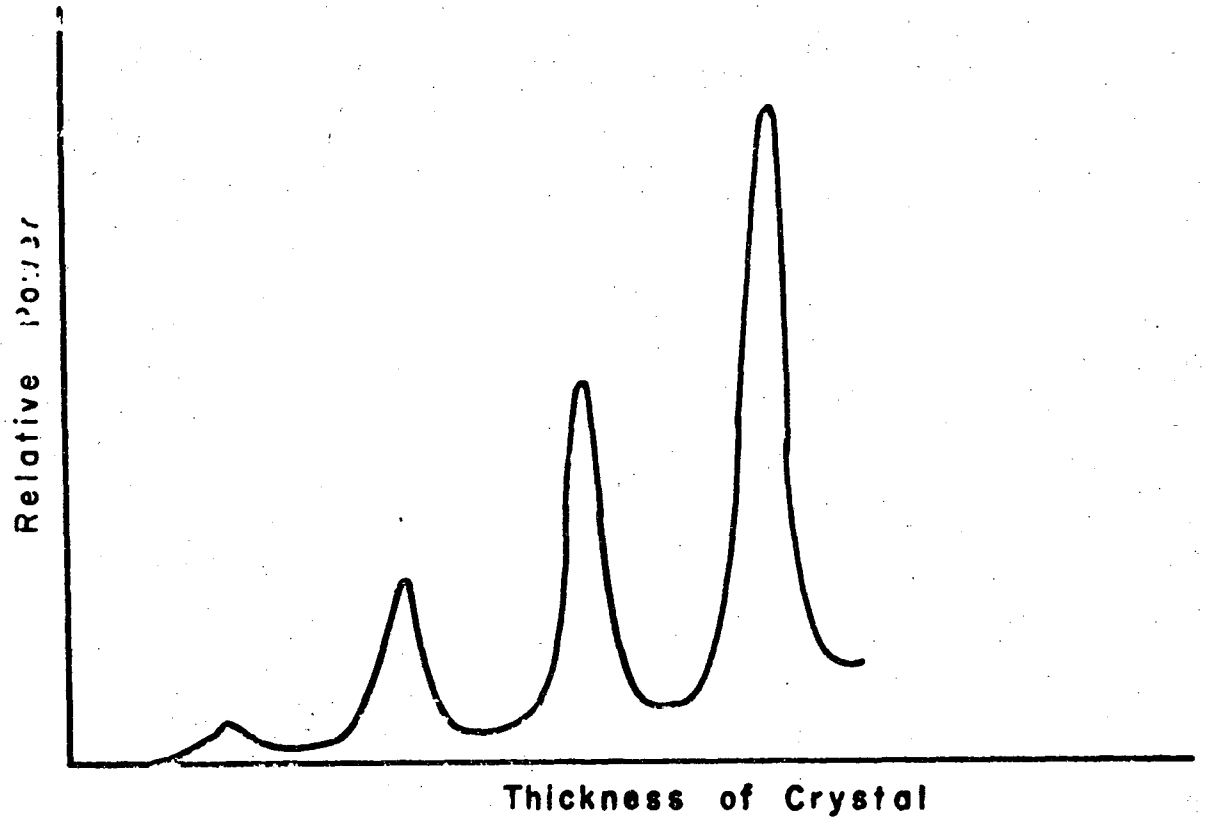

XBL 698-1130

Fig. 19 Effect of Boundary Conditions in $LiNbO_3$ (Theoretical). The peaks of output power occur at intervals of $\lambda/2$, where λ is the wave length in the medium. Experimentally, diffuse reflections from transverse boundaries and lack of monochromaticity decrease the depth of modulation.

$e^{-\alpha\ell} \sim 9$ for $\ell = 1.5$ cm lowers the effective reflectivity $r_{eff}^2 = r^2 e^{-\alpha\ell}$ cutting the modulations to about 20%. Moreover, 1.5 cm contains about 150 half-wave lengths; thus the angle of collection is large enough, about 0.076 radians measured inside the crystal, to average over a large fraction of a modulation cycle. This corresponds to the shrinking of Fabry-Perot rings as the spacing is increased until more than the central spot enters the detection system. For the 0.047 cm crystal, 8.1 cm^{-1} coincidentally falls on a peak, representing 5 half-wave lengths. The peak is about 3 times an average value. Thus the expected ratio for simple plane-waves would be expected to be reduced by a factor 3 if we hit a peak in the thin crystal. Experimentally, this did not materialize. We should be able to change the temperature of one laser, thus scanning the wave length, and find factors of 10 in variation. We find variations by a factor of 2. One reason is the lack of monochromaticity. Several wave lengths separated by 0.2 cm^{-1} cannot all appear at a peak. Thus the variation should be less than a factor of 10, perhaps 5. The further reduction may be due to diffuse reflections at the edges of the crystal. The existence of the peaks and instability in frequency may have been responsible for variations of a factor of 2 in the normalization scheme using thin crystals. The normalization was considerably better for crystals where length or absorption averaged out this effect.

The absorption is seen already to have an effect involving the boundary conditions [Eq. 10]. It also appears in Eq. (8). Qualitatively, absorption of the far infrared radiation limits the effective length for generation to the last absorption length of the crystal; any

radiation generated before this is absorbed. Combining Eq. (8) and Eq. (10), $\alpha = 1.4$ cm^{-1} yields a value for the power generated in the 1.5 cm crystal four times smaller than for $\alpha = 0$ cm^{-1}, averaged over the effects of the boundary conditions. This is a reasonable number, since the absorption length, $1/\alpha$, is about half of the length of the crystal. The effect of absorption in the 0.047 cm crystal is small.

Another possible reduction in power output in a longer crystal is due to the birefringence. Birefringence causes double refraction, causing two finite beams to "walk-off" from each other, limiting the distance over which the beams may overlap. An alternative viewpoint is this: Finite beams have an angular spread due to diffraction. Birefringence causes the index of refraction to change with direction; thus different parts of the beam have different indices of refraction. The result is that only one part of the beam can have perfect phase-matching and the length of interaction for various parts of the beam is limited by the lack of perfect phase-matching. However one wishes to interpret it, the effect is included in our calculations [Eq. 18] in the appearance of the variable ζ. Let us assume the modes of the lasers have a divergence half-angle of 2 mrad [intensity falls to e^{-2} times peak intensity] and propagate 50 cm before striking the crystal interface. The resultant radius at the laser output is $w_o = 0.011$ cm and at the crystal $w_o(1 + \xi^2)^{1/2} = 0.1$ cm, ξ being equal to 9. The factor, ζ, defined in Eq. 14 and calculated at the phase-matching angle, is equal to 0.0122. For a given Fourier component of the polarization wave, the dependence on ζ appears in Eq. (18) as

$\exp\left[-\frac{\zeta^2 z'^2}{2w_o^2} - \frac{k_x \zeta z' \xi}{2}\right]$. It is apparent that for $\zeta z' \sim w_o$, i. e., crystals on the order of 1 cm long with the beam described above, there is a sizable effect. The effect on the total power output, obtained by integration on z', k_x, and k_y, is not clear because of complexity of the function. A computer calculation for our experimental situation (1.5 cm $LiNbO_3$ and the beam described above) showed little change in total power from the case of $\zeta = 0$. The reason can perhaps be seen by rewriting the entire exponential of Eq. (18) in the following form:

$$\exp\left[-\frac{\zeta^2 z'^2}{2w_o^2(1+\xi^2)} - \frac{k_y^2 w_o^2(1+\xi^2)}{8} - 1/8\left(k_x + \frac{2\zeta z'\xi}{w_o^2(1+\xi^2)}\right)^2 w_o^2(1+\xi^2)\right].$$

In the first term, there is a sizable effect when $\zeta z' \sim w_o(1+\xi^2)^{1/2}$. In our case, $\zeta z' \ll w_o(1+\xi^2)^{1/2}$. The appearance of ζ in the last term represents a shift of the intensity distribution along the k_x direction. The shift is appreciable if $\zeta z'\xi \gtrsim w_o (1+\xi^2)^{1/2}$. The total collected power would be different if the shifted components are not phase-matched or they produce radiation outside the collection cone. The shift is also dependent on z', making its overall effect on the total power difficult to estimate. For our case, this effect is apparently small. It should be mentioned that $\zeta \to 0$ as $\theta \to 0$ $^{\pi}/2$ [Eq. 14]. This has been used in second harmonic generation to avoid the birefringence effect. Temperature variation of the refractive indices is used for phase-matching at $\theta = {}^{\pi}/2$.[51]

In both Eq. (18) and Eq. (6), we recognize that the angular dependence of the output will take the form of the diffraction of the

polarization source. For the single mode of 2 mrad divergence assumed above, the angle at which the amplitude of $P(k_T)$ falls to $P(o)/e$ for 8.1 cm^{-1} radiation is 4.9° from the beam axis inside the crystal. Radiation at 4.9° from the normal to the crystal interface is refracted to an angle of 34° outside the crystal. Thus we should expect a half-angle divergence of 34° for the radiation produced, provided the entire range of angles is sufficiently well phase-matched. The phase mismatch we are concerned with here is not a mismatch due to variation of refractive indices with angle. It is a mismatch due to noncollinearity: the far infrared radiation emerges at an angle Φ with respect to the laser beam. This is illustrated in Fig. 20, the functional form being identical to the mismatch in η of Eq. (6). For a 1.5 cm $LiNbO_3$ crystal and $\Delta k(0) = 0$, η corresponding to the 4.9° mentioned above is $\pi/4$, $\left(\frac{\sin\eta}{\eta}\right)^2 \approx 0.8$. Thus there is little decrease in power output in this crystal due to phase-mismatch and the angular spread of the output should be very close to the diffraction pattern of the polarization source.

The variation of the far infrared power as the 1.5 cm $LiNbO_3$ crystal is rotated through the phase-matched direction is shown in Fig. 15. The experimental points are compared with the $\left(\frac{\sin\eta}{\eta}\right)^2$ curve plotted assuming that the output of each laser is split equally between two frequencies separated by 0.2 cm^{-1}. Since the peaks are resolved, the peak power should be down by a factor of 2 from that calculated above for single frequency inputs. The position of the peak in Fig. 15 agrees within experimental accuracy with the phase matching angle of 9.5° from the optic axis computed using $n_e = 2.189$ and $n_o = 2.273$ (at

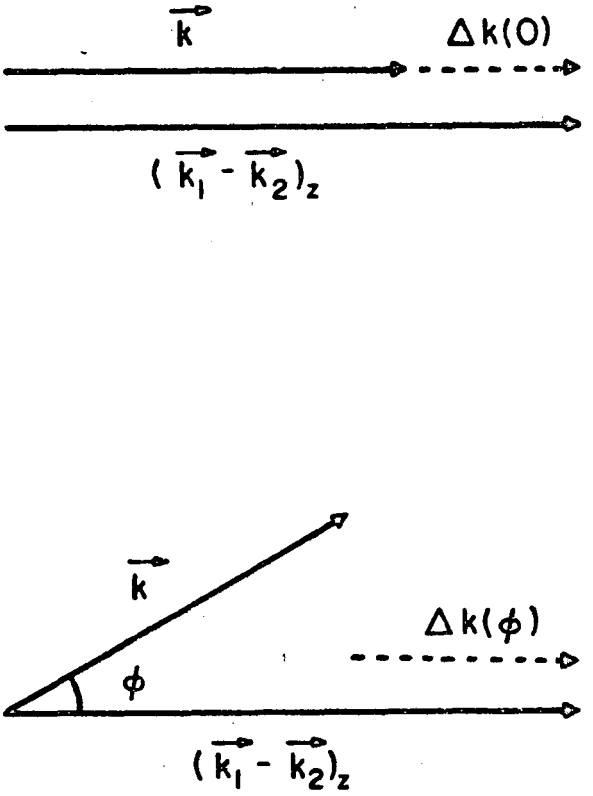

XBL 698-1131

Fig. 20 Phase Mismatch Due to Noncollinearity. The upper figure shows the collinear mismatch, with laser wave vectors given by $k_1 = \frac{\omega_1}{c} n_o$ and $k_2' = \frac{\omega_2}{c} n_e$ and the difference frequency wave vector given by $k = \frac{\omega_1 - \omega_2}{c} n_{ir}$. The lower figure shows an additional mismatch due to noncollinearity $\Delta k(\Phi) = \Delta k(0) + k(1 - \cos\Phi)$. Boundary conditions require Δk to be in the z-direction.

the laser frequencies)[52] and $n_o = 6.55$ (at 8.1 cm^{-1}).[49] It has been suggested that effects which decrease the power below that of the simple theory, effects such as absorption, double refraction, and optical inhomogeneities in the crystal, must simultaneously broaden the phase matching curve. This is not strictly true. Let us consider the plane-wave solution of a single Fourier component as an illustration. The phase-matching curve is given by the power as a function of the mismatch Δk (see Eq. 7)

$$W(\Delta k) \propto \left| e^{-(\alpha/2)\ell} \int_0^\ell P_1(z)\, e^{i\Delta kz}\, e^{(\alpha/2 - \alpha_L)z}\, dz \right|^2 . \qquad (19)$$

For $P_1(z)$ constant and $\alpha/2 = \alpha_L = 0$, we get the familiar $\left(\frac{\sin \eta}{\eta}\right)^2$ form. It is also apparent that decreasing P_1, keeping it constant, or increasing α, α_L, maintaining $\alpha/2 = \alpha_L$, can decrease the power by any arbitrary amount without changing the phase-matching curve. Physically, the absorption of the laser means a decrease in contributions to the output as we progress through the crystal; the nonlinear polarization decreases as the laser is absorbed. Absorption of the far infrared radiation means an increase in contributions to the output as we progress through the crystal; the radiation produced near the entrance face of the crystal is absorbed more than that produced near the exit face. The result is that Eq. (19) again involves a Fourier transform of a constant function from 0 to ℓ.

Generally, the special conditions above are not applicable. An effect such as absorption would decrease the effective length, making the Fourier transform and thus the phase-matching curve broader. However, the change is slow. The absorption length $1/\alpha$ must be several

times shorter than the crystal length before the width at half maximum changes significantly. A concrete example is shown in Fig. 16. This can be understood as follows. The phase-matching curve for an exponential function with a full width of ℓ at e^{-1} of the maximum value has a width at half maximum of $1.25/\ell$ compared to $2.8/\ell$ for the phase-matching curve of a constant function from 0 to ℓ. For the phase-matching curves to be equally broad in the two cases, the effective length of the medium in the exponential case can be reduced by a factor of 2. There is a considerable effect on the tails of the curves and good experiments should show this.

We may summarize the above as follows: Using the simple monochromatic plane-wave solution gives a ratio of 1000:1 for the output of the 1.5 cm crystal to that of the 0.047 cm crystal. Including the effect of absorption reduces the ratio by a factor of 4. Including the effect of boundary conditions reduces it further by a factor of 3. (This factor is in doubt because of inability to see large variations in the 0.047 cm crystal with change in frequency.) A further reduction of a factor of 2 occurs because several frequency modes cannot all phase-match in the longer crystal. Effects of beam divergence because of birefringence or noncollinear phase mismatch are not very large. Further reductions must be attributed to the problems mentioned earlier, such as optical inhomogeneities and misalignment of the two lasers.

Typical far infrared wave length measurements are shown in Fig. 17 as Fabry-Perot transmission curves. The solid curves are obtained from the Airy formula by integrating over the finite collection angle so as to fit the decrease in Q with increasing order number. The assumed

collection half-angle was 30°. It must also be assumed that the angular spread of the output is this large, or larger. This is in accord with our estimate above and is confirmed experimentally by the fit of these curves and by crude measurements of the angular variation which indicate considerable output at angles up to 30°. The finesse was computed from the geometry of the mesh. The wave lengths used for the fit were within a few percent of those predicted by the known temperature dependence of the ruby laser frequency. The fit shows unambiguously that we are observing a difference frequency with a bandwidth less than the ~ 1 cm^{-1} resolution of the interferometer. The linewidth of the two frequency modes from each laser is less than 0.02 cm^{-1}, leading to a predicted linewidth of less than 0.04 cm^{-1} for each of the three far infrared frequencies produced.

Using a 0.3 cm $LiNbO_3$ crystal, the temperature difference was lowered to determine the minimum frequency we could produce and detect. We were able to detect radiation at $\Delta T = 9°C$, corresponding to 1.2 cm^{-1} radiation. We were thus able to cover the range from 1.2 cm^{-1} to 8.1 cm^{-1}, the high frequency limit being determined by our temperature-control system.

By using one laser at the R_1-transition, the other laser at the R_2 transition and varying the temperature difference we can produce radiation from 21 cm^{-1} to 37 cm^{-1}. Examples are shown in Fig. 18 by the Fabry-Perot wave length measurements. It will be noticed that the effect of averaging over angles seen in Fig. 16 is absent. This is because the wave lengths are shorter by a factor of about 4, giving a narrower angular divergence by about the same factor. This gives a

divergence half angle of 9° outside the crystal.

The phase-matching curve for production of the difference frequency at 29 cm^{-1} is shown in Fig. 16. The crystal thickness is 0.15 cm and the absorption coefficient[50] α is 18 cm^{-1}. The theoretical curve for no absorption is shown for comparison. The width at half-maximum is changed very little while the wings show a definite effect.

The peak power for this case was about 5 milliwatts compared to the 1 milliwatt for 8.1 cm^{-1} in the 0.047 cm crystal. Since the absorption length at 29 cm^{-1} is about equal to the crystal length used for 8.1 cm^{-1} generation and we are in the regime of collecting the entire angular spread, implying ω^2 dependence of power on frequency, we could guess that the power at 29 cm^{-1} should be about 15 times the power at 8.1 cm^{-1}. Computer calculations give a factor of 12. Since the power of the R_2-transition laser is reduced by a factor of about two from its power in the R_1-transition, we should expect a factor of 6 compared to the factor of 5 observed. In view of the difficulties in both calculations and experiments, this agreement must be considered fortuitous.

We also compared the far-infrared power generated from a 1 cm thick crystal of quartz to that from the 0.047 cm $LiNbO_3$ crystal. From this measurement we estimate the ratio of the electro-optic coefficients $r_{22}(LiNbO_3)$: r_{62}(quartz) to be 8.5. According to other measurements,[53] the ratio is 3.7. This must be considered satisfactory agreement.

C. Discussion

Opportunities for further research in this area are numerous. Primarily, the need is for better and more versatile experiments. Possible improvements include the following: (1) more sensitive and/or faster far infrared detectors, (2) improvements in quality and choice of nonlinear crystals, (3) improvements in the laser sources, (4) use of other laser or non-laser sources, and (5) use of other configurations, e.g. non-collinear phase-matching.

With increased demand for optical quality crystals of many different materials, there has been considerable improvement in crystal quality. The considerable amount of work in electro-optics gives us the nonlinear susceptibility for low frequencies for many substances. The far infrared absorption spectra is not as widely studied and is important to know. Much work needs to be done in studying the properties which result in high difference-frequency power outputs. An ideal crystal would be transparent to the lasers and the far infrared, have large nonlinear susceptibilities, be easily obtainable in good quality large crystals, be highly resistant to optical damage, and be phase-matchable.

Improvements in the laser sources, particularly the divergence, should produce significant increases in power. If the spatial coherence of the laser sources is good enough to make the divergence of the far infrared output less than the divergence which the collection system can handle, we can increase the power by choosing the optimum focusing of the lasers into the crystal, provided that the crystal can withstand the higher powers. Consideration of Eq. (18) can give us the basic

ideas. The coefficient $\frac{\chi E_{\omega_1} E^*_{\omega_2} w_o^2}{2}$ remains constant upon increased focusing, i. e., decreasing w_o. The area πw_o^2 decreases and the intensity $|E|^2$ increases to make the energy passing a given plane constant. Along with decreasing w_o, we get an increase in angular spread, i. e., larger k_T are allowed before the exponential cuts off. Thus, with the coefficient remaining constant, we would expect an increase in power proportional to the increase in divergence solid angle, i. e., proportional to $\frac{1}{w_o^2}$, until other effects begin to cut the generation of far infrared radiation. The angular cutoffs are the collection angle and the lack of phase-matching due to non-collinearity, expressed in Eq. (6). There is an angular dependent phase mismatch due to the birefrigence (the term $\exp\left(\frac{ik_x \zeta z'}{2}\right)$) but this term, with ζ typically less than 0.01, is always less important than the non-collinear phase mismatch. The z-dependence of $P(k_T,z)$ reveals two effective lengths which also may cut off the expected increase in power, provided they become shorter than the crystal or absorption length. They are the Rayleigh range, $z_R = \frac{1}{2} k_L w_o^2$, k_L being the laser wavevector, and a characteristic length depending on the birefringence, $\ell_\zeta = \frac{w_o}{\zeta}$. The Rayleigh range is an effective length of the focal region and appears in Eq. (18) in the dependence on ξ; an increase in $|\xi|$ means movement away from the focal point, a larger, less intense beam, and a resultant decrease in the angular divergence. The characteristic length ℓ_ζ represents the distance of significant overlap of the extraordinary and ordinary beams.

The regions of importance of these effects should at least be mentioned. Assuming $\zeta \sim 0.01$, $\ell \sim 1$ cm (crystal thickness), ℓ_ζ and z_R

being on the order of the length of the crystal implies $w_o \sim 0.01$ and thus a divergence of the output for frequencies $\bar{\nu} \lesssim 100\ cm^{-1}$ greater than the collection cutoff of 30°. Noncollinear phase mismatch (Fig. 20) causes a cutoff at smaller angles than 30° for $\bar{\nu} > \frac{8n}{\ell}\ (cm^{-1})$, n being the far infrared refractive index. Thus for $\bar{\nu} \lesssim 100\ cm^{-1}$ and the crystal considered here, either the collection or phase-matching cutoff is the limiting factor in increasing power by focusing. This is only an instructive <u>particular</u> example and the conclusions should not be indiscriminately applied.

The range of tunability of the ruby lasers is quite limited. Other systems should be better. One possibility is stimulated Raman scattering of ruby laser frequencies. Using various liquids and temperature tuning the ruby laser sources would provide considerable tunability. The disadvantages are considerable loss of power and broadened linewidths. A system using two dye lasers would be tunable over the entire far infrared region. The power, linewidth, and divergence will perhaps never be as good as the ruby laser, but they may be quite adequate.

Professor Y. R. Shen has suggested the use of a mode-locked neodymium laser, whose linewidth is on the order of 100 cm^{-1}. The spectral output is a series of lines, spaced by $\frac{1}{2\ell}\ cm^{-1}$ where ℓ is the length of the laser cavity. There is ideally a fixed phase relationship between all the lines (all are in phase at some time), resulting in a temporal output of a series of sharp pulses, separated in time by $2\ell/c$. The total energy and overall time duration are comparable to ruby lasers. Thus each of the N spectral lines has about $1/N$ times the power of a typical ruby laser, a given pair producing difference frequency

powers down by the factor $1/N^2$. However, if our difference frequency is not near the extreme difference frequency possible with the given bandwidth, there are on the order of N pairs producing the same difference frequency in phase, cancelling the $1/N^2$ factor. Thus in the ideal case, the power for a given difference frequency line would be comparable to the power produced by two beating ruby lasers. Moreover, all difference frequencies which are phase-matchable would be produced at comparable power levels. The mode-locking is not ideal and this estimate is thus expected to be an order of magnitude or so too large. Nevertheless, this system shows great promise.

An example of other possible configurations is a simple non-collinear phase matching configuration. The primary advantage here is the ability to use crystals without birefrigence. An additional feature is an increased sensitivity of the phase-matching to divergence. The phase mismatch due to a given angular deviation or divergence of one of the lasers is proportional to sin Φ cos Φ where Φ is the angle between the far infrared wave vector and the laser beam wave vector. The power will thus be decreased for noncollinear phase-matching because various parts of the divergent laser beams will not phase-match. The output would be more collimated.

ACKNOWLEDGMENTS

I would like to thank the following people for their part in this work:

My wife, Sally, for her continual support throughout the work;

Professor Y. R. Shen, for his patience, perseverance, and sure-handed guidance of the research;

Professor P. L. Richards, for his enthusiastic support and invaluable assistance;

Dr. Karl Gehring and Patrick Yang, for their work on far-infrared detection and crystal preparation as well as numerous discussions;

Kathy Williams, for typing the entire manuscript;

Jim Morris, for reading the manuscript and making useful suggestions.

This work was performed under the auspices of the Office of Naval Research and the U. S. Atomic Energy Commission.

REFERENCES

1. N. Bloembergen, Nonlinear Optics (W. A. Benjamin, Inc., New York, 1965).

2. A. Yariv, Quantum Electronics (J. Wiley, New York, 1967).

3. D. H. Martin, Spectroscopic Techniques for Far Infrared, Submillimeter and Millimeter Waves, D. H. Martin (editor), (North-Holland Publishing Co., Amsterdam, 1967).

4. First observed by P. A. Franken, A. E. Hill, C. W. Peters, G. Weinreich, Phys. Rev. Letters, 7, 118 (1961). There exists much literature on the subject since then.

5. M. Bass, P. A. Franken, J. F. Ward and G. Weinreich, Phys. Rev. Letters 9, 446 (1962).

6. J. A. Giordmaine, Phys. Rev. Letters 8, 19 (1962).

7. P. D. Maker, R. W. Terhune, M. Nisenoff, and C. M. Savage, Phys. Rev. Letters 8, 21 (1962).

8. K. E. Niebuhr, Appl. Phys. Letters 2, 136 (1963).

9. A. W. Smith and N. Braslau, IBM Journal Res. 6, 361 (1962).

10. See, for example, D. C. Lainé, Nature 191, 795 (1961).

11. F. Zernike, Jr. and P. R. Berman, Phys. Rev. Letters 15, 999 (1965).

12. T. Yajima and K. Inoue, Physics Letters 26A, 281 (1968) and IEEE J. Quantum Electron. QE-5, 140 (1969).

13. F. Zernike, Bull. Am. Phys. Soc. 12, 687 (1967).

14. N. Van Tran and C. K. N. Patel, Phys. Rev. Letters 22, 463 (1969).

15. T. H. Maiman, Phys. Rev. Letters, 4, 564 (1960).

16. I. D. Abella and H. Z. Cummins, J. Appl. Phys. 32, 1177 (1961).

17. D. E. McCumber and M. D. Sturge, J. Appl. Phys. 34, 1682 (1963).

18. N. Kumagai, M. Matsuhara, H. Mori, IEEE J. Quantum Electron. QE-1, 85 (1965).

19. D. A. Kleinman, P. P. Kisliuk, Bell Syst. Tech. J. 41, 453 (1962).

20. T. R. Koehler, J. P. Goldsborough, Bull. Amer. Phys. Soc. 7, 446 (1962).

21. D. Roess, Proc. IEEE (Correspondence) 52, 196 (1964).

22. For a bibliography, see the series of laser bibliographies by K. Tomiyasu, the most recent being J. Quantum Electronics QE-4, 274 (1968).

23. M. Bass, P. A. Franken, A. E. Hill, C. W. Peters, G. Weinreich, Phys. Rev. Letters 8, 18 (1962).

24. B. H. Soffer and B. B. McFarland, Appl. Phys. Letters 8, 166 (1966).

25. D. W. Gregg and S. J. Thomas, J. Appl. Phys. 37, 3750 (1966).

26. N. Van Tran and D. Kehl, Appl. Optics 5, 168 (1966).

27. S. Sugano and Y. Tanabe, J. Phys. Soc. Japan 13, 880 (1958).

28. F. J. McClung, S. E. Schwarz, and F. J. Meyers, J. Appl. Phys. 33, 3139 (1962).

29. C. J. Hubbard and E. W. Fisher, Appl. Optics 3, 1499 (1964).

30. J. A. Calviello, E. W. Fisher, and Z. H. Heller, IEEE J. Quantum Electronics (Correspondence) QE-1, 132 (1965).

31. B. Lyot, Compt. Rend. 197, 1593 (1933).

32. Y. Öhman, Nature 141, 291 (1938).

33. M. Maier, W. Kaiser and J. A. Giordmaine, Phys. Rev. Letters 17, 1275 (1966).

34. J. A. Armstrong, Appl. Phys. Letters 9, 72 (1966).

35. E. H. Putley and D. H. Martin in Ref. 3.

36. D. A. Kleinman, Phys. Rev. 126, 1977 (1962).

37. Y. R. Shen, Phys. Rev. 167, 818 (1968).

38. See Ref. 2, Appendix 3, p. 459.

39. See, for example, I. P. Kaminow and E. H. Turner, Appl. Optics 5, 1612 (1966).

40. See, for example, C. G. B. Garrett, IEEE J. Quantum Electronics QE-4, 70 (1968).

41. P. P. Bey, J. F. Giuliani, H. Rabin, Phys. Rev. Letters 19, 819 (1967).

42. J. E. Bjorkholm, Phys. Rev. 142, 126 (1966).

43. D. H. McMahon and A. R. Franklin, Appl. Phys. Letters 6, 14 (1965).

44. G. D. Boyd and J. P. Gordon, Bell System Tech. J. 40, 489 (1962).

45. G. D. Boyd and H. Kogelnik, Bell System Tech. J. 41, 1347 (1962).

46. G. D. Boyd, W. L. Bond, and H. L. Carter, J. Appl. Phys. 38, 1941 (1967).

47. A. Ashkin, G. D. Boyd, J. M. Dziedzic, R. G. Smith, A. A. Ballman, J. J. Levinstein, and K. Nassau, Appl. Phys. Letters 9, 72 (1966).

48. R. L. Byer, Stanford Microwave Laboratory Report No. 1711, p. 127 (1968).

49. J. D. Axe and D. F. O'Kane, Appl. Phys. Letters 9, 58 (1966).

50. D. R. Bosomworth, Appl. Phys. Letters 9, 330 (1966) and J. G. Bergman, A. Ashkin, A. A. Ballman, J. M. Dziedzic, H. J. Levinstein, and R. G. Smith, Appl. Phys. Letters 12, 92 (1968).

51. R. C. Miller, G. D. Boyd and A. Savage, Appl. Phys. Letters 6, 77 (1965).

52. G. D. Boyd, R. C. Miller, K. Nassau, W. L. Bond, and A. Savage, Appl. Phys. Letters 5, 234 (1964).

53. See Ref. 2, p. 351.

54. In calculating H for the boundary condition, $\frac{df}{dz}$ is neglected. This corresponds to neglecting fields generated in a boundary layer of thickness $\frac{\lambda}{2\pi}$, where λ is the far infrared wavelength in the medium. Thus the calculation is valid for transmitted fields if the thickness of the crystal is several wavelengths.

LEGAL NOTICE

This report was prepared as an account of Government sponsored work. Neither the United States, nor the Commission, nor any person acting on behalf of the Commission:

A. Makes any warranty or representation, expressed or implied, with respect to the accuracy, completeness, or usefulness of the information contained in this report, or that the use of any information, apparatus, method, or process disclosed in this report may not infringe privately owned rights; or

B. Assumes any liabilities with respect to the use of, or for damages resulting from the use of any information, apparatus, method, or process disclosed in this report.

As used in the above, "person acting on behalf of the Commission" includes any employee or contractor of the Commission, or employee of such contractor, to the extent that such employee or contractor of the Commission, or employee of such contractor prepares, disseminates, or provides access to, any information pursuant to his employment or contract with the Commission, or his employment with such contractor.

TECHNICAL INFORMATION DIVISION
LAWRENCE RADIATION LABORATORY
UNIVERSITY OF CALIFORNIA
BERKELEY, CALIFORNIA 94720